FR 9103191

I.P.N. BP n°1 – 91406 ORSAY

institut de physique nucléaire CNRS - IN2P3 - UNIVERSITÉ PARIS - SUD

48 pages

DECAYS OF ^{181}Hg ($T_{1/2}$=3.6s) AND ^{181}Au ($T_{1/2}$=11.4s)
LOW-SPIN STATES OF ^{181}Pt AND ^{177,181}Ir

J.Sauvage, C.Bourgeois[1], P.Kilcher, F.Le Blanc, B.Roussière
Institut de Physique Nucléaire, 91406 Orsay, France
M.I. Macias-Marques
Centro de Fisica Atomica,
Universidade de Lisboa, 1699 Lisboa, Portugal
F. Bragança Gil
Centro de Fisica Nuclear, 1699 Lisboa, Portugal
M.G. Porquet
ntre de Spectrométrie Nucléaire et de Spectrométrie de Masse
91405 Orsay, France
H. Dautet
Foster Radiation Laboratory, Mc Gill University,
Montréal, Québec, Canada H3A 2B2
and the ISOCELE Collaboration

IPNO-DRE 90-11

DECAYS OF ^{181}Hg ($T_{1/2}$=3.6s) AND ^{181}Au ($T_{1/2}$=11.4s)
LOW-SPIN STATES OF ^{181}Pt AND ^{177,181}Ir

J. Sauvage, C. Bourgeois[1], P. Kilcher, F. Le Blanc, B. Roussière
Institut de Physique Nucléaire, 91406 Orsay, France

M.I. Macias-Marques
Centro de Fisica Atómica,
Universidade de Lisboa, 1699 Lisboa, Portugal

F. Bragança Gil
Centro de Fisica Nuclear, 1699 Lisboa, Portugal

M.G. Porquet
Centre de Spectrométrie Nucléaire et de Spectrométrie de Masse
91405 Orsay, France

H. Dautet
Foster Radiation Laboratory, Mc Gill University,
Montréal, Québec, Canada H3A 2B2

and the ISOCELE Collaboration

Abstract : The decay of ^{181}Au ($T_{1/2}$=11.4s) has been investigated using mass-separated radioactive sources produced by the ISOCELE facility. Level schemes of ^{177}Ir, ^{181}Ir and ^{181}Pt have been obtained. Most of the levels located at low excitation energy in ^{181}Ir and ^{181}Pt are identified as states corresponding to prolate-shaped nuclei. However the highly-converted transitions observed in ^{181}Pt could indicate a new region of shape transition in the very neutron-deficient platinum isotopes.

RADIOACTIVITY ^{181}Hg, ^{181}Au [from Pt(^{3}He,xn)Hg, Pt(p,xn)Au, on-line mass separation] ; measured E_α, I_α, E_γ, I_γ, I(ce), $\alpha\gamma$t-, $\gamma\gamma$t-coin ; ^{177}Ir, ^{181}Ir, ^{181}Pt deduced levels, J, π, ICC, γ-multipolarity, highly-converted transitions. Hyperpure Ge, Si (Li), mini-orange magnetic filter.

[1] and Laboratoire de Physique Nucléaire, Université Paris VII, 75251 Paris, France.

1. Introduction

The platinum isotopic series is in the middle of the transitional region situated between the well-deformed rare-earth nuclei and the spherical doubly magic nucleus ^{208}Pb. Many experimental [1-17] and theoretical [18-27] studies have already been performed on these nuclei. They have soft potential energy surfaces [22,24] and dynamical effects are expected to be important [25,26]. Studies of the variation of the mean-square charge radius $\delta\langle r^2\rangle$ indicate that the radius stays almost constant when the mass decreases from 191 to 186 [refs. [14,17,28]]. A transition from an oblate or more likely triaxial shape for platinum isotopes with A>186 to a prolate deformation for the ^{185}Pt nucleus has been established clearly [14]. However, this shape transition results in a small increase in the charge radius r_c whereas the shape change observed in the Hg and Au isotopes leads to a drastic increase in r_c values [29-32]. Recent studies by radioactivity and (HI,xnγ) reactions have shown that the low excitation energy levels of ^{183}Pt and ^{185}Pt can be interpreted as Nilsson states corresponding to prolate-shaped nuclei [12,16,33,34]. On the other hand, highly-converted transitions have been observed in $^{185,187}Pt$ [refs. [4,6,7,12]] but not in ^{183}Pt [ref. [16]]. ^{185}Pt and ^{187}Pt are both located close to the shape transition, and shape coexistence in ^{187}Pt has been suggested by M.C. Abreu et al. [35] from an in-beam experiment. In-beam studies have suggested that shape coexistence appears also in $^{176,178}Pt$ isotopes [10].

In order to search for shape coexistence and highly-converted transitions in the odd-A neutron-deficient platinum isotope ^{181}Pt, which is the first isotope below the middle of the neutron shell N=104, we have investigated the β^+/EC decay of ^{181}Au. The short half-lives of ^{181}Au and ^{181}Pt have also led us to study the β^+/EC decay of ^{181}Pt since γ-rays belonging to this decay were also observed in the spectra. Preliminary results concerning the identification of the main γ-lines emitted in the $^{181}Au \rightarrow {}^{181}Pt$ decay have already been published [36] and the $^{181}Pt \rightarrow {}^{181}Ir$ and $^{181}Au \rightarrow {}^{177}Ir$ decay have previously been studied [37-39]. During the course of the present work, high-spin states of ^{181}Pt have been investigated by (HI,xnγ) reactions [40]. This latter experiment, in addition to our own, sheds light on some ambiguous experimental results.

In this paper, we will first present the experimental results concerning the decay of ^{181}Au . Then the levels observed at low excitation energy will be identified as Nilsson states. Lastly the presence of highly-converted transitions in ^{181}Pt and ^{181}Ir will be discussed.

2. Experimental procedures

Radioactive sources of ^{181}Au were produced either directly or from the β^+/EC decay of ^{181}Hg. Transitions in ^{181}Pt have been studied using both possibilities to define the best experimental conditions. In order to produce ^{181}Au or ^{181}Hg nuclei, a 7 gram Pt-B alloy target [41,42]) placed inside the ion source of the ISOCELE separator [43]) was irradiated either by the 200 MeV proton beam ($I \sim 2\mu A$), or by the 270 MeV ^3He beam ($I \sim 2\mu A$), from the Orsay synchrocyclotron. The yield was sufficient (around 10^5 atoms/s) in both cases to allow us to study the ^{181}Au decay. However, as the γ spectra were highly complex, we chose to mainly study the decay of the ^{181}Au nuclei directly produced by Pt(p,xn)Au reactions. The mass-separated radioactive ions were collected on a mylar-aluminum tape and the radioactive sources obtained were moved at regular intervals in front of a counting set-up. First, to accurately determine the energies of the γ-rays, the ^{181}Au sources were simultaneously counted with a ^{226}Ra source. The corresponding γ-rays were detected using two Ge(HP) N-type coaxial detectors (resolution 1.9 keV FWHM at 1.33 MeV and 18% efficiency), one covering an energy range from 10 keV to 1.5 MeV, the other from 40 keV to 4.6 MeV. Then, singles γ-rays were obtained using the same two detectors but with an energy range from 10 keV to 1.5 MeV for one of the detectors and from 20 keV to 2.4 MeV for the other. A total of 5.10^7 γ-γ-t coincidence events were recorded in event-by-event mode on the magnetic tape driven by a PDP 11-34 computer. The α-particles emitted by the decay of the ^{181}Au nuclei were detected by a silicon surface barrier detector and α-γ-t coincidence events were also recorded in event-by-event mode. Singles γ-ray spectra were analysed using SAMPO curve-fitting code [44]). The coincident events were collected in coincidence bidimensional matrices which were treated with the

MILFEUIL program [45]) working on the VAX 8530 computer at Orsay.

In order to determine the multipolarity of the main transitions, γ rays and conversion electrons were simultaneously detected by a Ge(HP)N-type detector and a cooled Si(Li) detector coupled to a mini-orange spectrometer. This type of spectrometer consists of a magnetic filter positioned between the source and the detector. Fig.1-a presents schematically the system used during this work. The toroidal magnetic field created by the permanent magnets (in this case 4 flat rectangular $SmCo_5$ magnets) bends the positrons outwards and the electrons towards the Si(Li)detector, while the electromagnetic radiation is stopped in the lead absorber. This leads to a strong suppression of the background and a much improved electron spectrum.

The transmission depends on the energy of the incident electrons, and the shape of the transmission curve is strongly influenced by the filter's parameters [46,47]). For this experiment they were chosen to yield a transmission curve as broad and flat as possible. This can be observed in fig.1-b which displays the relative efficiency curve of the spectrometer (transmission efficiency multiplied by detector efficiency). This curve has been determined (from 60 keV to 2.2 MeV) using the γ and electron lines observed in the decay of the ^{188}Pt and ^{188}Ir nuclei obtained from a mass-separated source of ^{188}Au produced by ISOCELE. For these measurements, spectra were analysed using the GAMANAM code [48]), a modified version of the GAMANAL curve-fitting code [49]).

Collecting and counting times for ^{181}Au sources were 10s for all of the measurements. Since the half-lives of ^{181}Hg, ^{181}Au and ^{181}Pt nuclei are respectively 3.6s, 11.4s and 51s [ref.[50])], lines belonging to the ^{181}Pt→^{181}Ir decay were present with high intensity in all the spectra. This allowed us to perform a partial study of the ^{181}Pt decay.

3. Experimental results

3-1 ^{181}Hg decay.

From the comparison of the γ spectra observed in the ^{181}Hg decay and ^{181}Au decay studies, we have deduced the γ-lines which can be assigned to the ^{181}Hg decay (see table 1). These γ-lines could belong either to the $^{181}Hg \rightarrow ^{181}Au$ decay or to one of the decays which follow the α-particle emission of ^{181}Hg (fig.2). The 147.8 and 214.1 keV γ-lines probably correspond to the de-excitation of the 147.4 and 214.2 keV levels which were previously established by Hagberg et al. [37] in ^{177}Pt. Nevertheless an important part of the intensity of the 147.8 keV line is likely due to the 148.4 keV γ-ray from the ^{177}Ir de-excitation (see next paragraph). Indeed, from the ^{181}Hg decay chain shown in fig.2, one can estimate that the number of ^{177}Ir nuclei produced through ^{177}Pt is twelve times larger than that produced through ^{181}Au.

3-2 ^{181}Au decay

3-2-1 α decay

Six α-lines have been observed : their energies and intensities are reported in columns 1 and 2 of table 2. The α-lines attributed to the ^{181}Au decay by E.Hagberg et al. [37] from a previous ^{181}Hg decay study are reported in columns 3 and 4 of table 2. In the present work, the measurements were more sensitive, since the ^{181}Au mass-separated sources were directly produced. Hagberg et al. [37] had observed the 148 and 265 keV γ-rays respectively in coincidence with the 5.480 and 5.365 MeV α-lines. In our experiment the coincidence between the 148.4 keV γ- ray (I=25) and the 5.462 MeV α-line was clearly observed but the other coincidence was not. The results lead to the α-decay scheme of ^{181}Au proposed in fig.3. It should be noted that some γ-rays which are listed in table 1 could de-excite the states established in ^{177}Ir. Only γ-X coincidence measurements performed with ^{181}Hg sources could confirm this.

3-2-2 β decays

From γ-X and γ-γ coincidence measurements performed on ^{181}Au sources, 79 γ-lines can be clearly attributed to the $^{181}Pt \rightarrow ^{181}Ir$ decay. Their energies and intensities are reported in table 3 together with the main coincident γ-rays. The other γ-lines observed in the singles-γ spectra very likely belong to the $^{181}Au \rightarrow ^{181}Pt$ decay : these are listed in table 4. Although the electron spectrum is very complex (fig.4), conversion coefficients could be calculated for about 60 transitions (table 5). In some cases conversion coefficients could be determined only globally for 2 or 3 transitions. Then either a multipolarity could be deduced for each of the transitions or the consistency of the results could be verified. Thus, for example, from the conversion in the L subshell, a multipolarity M1 could be attributed to both 402 keV transitions, one belonging to ^{181}Pt and the other to ^{181}Ir. It is worth noting that at least 9 highly-converted transitions have been found in the electron spectrum.

3-2-3 ^{181}Ir level scheme

From the results given in tables 3 and 5 a partial level scheme of ^{181}Ir was built (fig.5). Twenty six excited levels have been established. Of these, seven are new while the others are found to be in agreement with those given in ref. [38]). The ground state and the levels located at 24.9 and 112.2 keV have been interpreted as the $5/2^-$, $9/2^-$ and $1/2^-$ states associated to the $1/2^-$ [541] Nilsson state from systematics [39]). The E2 multipolarity found for the 112.2 keV transition supports the spin and parity values $I^\pi = 1/2^-$ assigned to the 112.2 keV level. In fig.5, we indicate the I^π values we could attribute to the ^{181}Ir levels. These are deduced from previous assignments to the first three states, the transition multipolarities reported in table 5, and the following two facts :

i) the 1309.2 keV γ-line (I_γ = 28) appears with intensity as strong as that of the 1407.8 keV γ-line (I_γ = 22) in the 230.2 keV coincidence spectrum. It is in coincidence with the 230.2 keV γ-ray through the 98.6 keV transition which therefore has a total intensity of at least 20 units. Since the 98.6 keV transition has a γ-intensity I_γ = 4, it cannot have an E1 multipolarity (α_{total}(E1)=0.4) but very likely is M1 or E2 (α_{total}(M1) = 7, α_{total}(E2) = 5). This implies that both the 342.4 and 440.8 keV levels have the same parity (positive).

ii) the E1 multipolarity of the 1407.8 keV transition implies a negative parity value for the 1750.1 keV level.

Therefore the 1309.2 keV transition which de-excites the 1750.1 keV state towards the positive-parity level located at 440.8 keV cannot have an M1 or E2 multipolarity, but very likely has an E1 multipolarity.

3-2-4 ^{181}Pt level scheme

The level scheme given in fig.6 has been established from the results listed in tables 4 and 5. From systematics the ground state and the 79.4, 94.0 and 278.2 keV levels had been previously identified as the $1/2^-$, $3/2^-$, $5/2^-$ and $7/2^-$ members of the rotational band built on the $1/2^-$ [521] Nilsson state [36,52,53]. The multipolarities determined in the present work support this identification, and the 300.9 keV level, which de-excites only towards the $5/2^-$ via an E2 transition, is very likely the $9/2^-$ member of this rotational band. The main γ-lines observed in coincidence with the 94.0 keV γ-ray are also observed with the 79.4 keV γ-ray. This implies that an unobserved 14.5 keV transition connects the 94.0 and 79.4 keV levels. Its total intensity can be estimated around 1800±300.

The 116.8 keV level is established from the coincidence observed between the 22.8 and 94.0 keV γ-lines. It has a long half-life ($T_{1/2}$ > 300 ns) since no γ-rays feeding it are seen in coincidence with the 22.8 keV line within the experimental timing requirements. Its spin value is very likely $\geqslant 7/2$. From the intensity balance of the 94.0 keV and 116.8 keV levels, the total intensity of the 22.8 keV must be between 1700 and 3800, which is only compatible with an M1 or M1+E2 multipolarity. This has led us to attribute spin and parity values $I^\pi = 7/2^-$ to the 116.8 keV level which could be then the $7/2^-$ [514] Nilsson state.

The 159.4 keV γ-line is observed in the γ-γ delayed-coincidence matrix and the half-life of the 276.2 keV level is estimated to be between 20 ns and 300 ns. The 159.4 keV transition very likely de-excites a $9/2^+$ level towards the $7/2^-$ [514] state. Its properties are quite similar to those of the 161.2 keV abnormal E1 transition which deexcites the $9/2^+$ [624] state to the $7/2^-$ [514] level in the ^{183}Pt level scheme [16]. The 40.5 keV γ-ray is clearly coincident with the 118.9 keV line and the sum of their energies is equal to 159.4 keV (see table 4). This suggests that the 40.5 - 118.9 keV cascade is located in parallel with the 159.4 keV transition. In the same way, the 120.6 keV γ-ray is coincident with the 50.0 keV line. The sum of their energies is very close to the energy of the 170.5 keV transition and several γ-rays are observed in coincidence with both the 120.6 and 170.5 keV γ-lines (see table 4). This indicates that the 120.6 - 50.0 keV cascade is located in parallel with the 170.5 keV transition. The order adopted for the two cascades has been determined from other coincidence relationships (see table 4 and fig.6). It is worth noting that from the intensity balance of the 235.7 keV level, the total intensity of the 40.5 keV transition has to be less than 300, which corresponds to a conversion coefficient α_{total} (40.5 keV)<4.6 and implies an E1 multipolarity for the 40.5 keV transition.

The 166.7 keV level which decays to the 116.8 keV $7/2^-$ state and also to the 5/2 and 3/2 members of the $1/2^-$ [521] rotational band is very likely the $5/2^-$ [512] state, which is expected to be located at low energy in ^{181}Pt. In addition its decay mode is very similar to that observed for the $5/2^-$ [512] state located at 367.4 keV in ^{183}Pt [ref.[16])].

The identification of the ground state, 116.8, 166.7 and 276.2 keV levels as the $1/2^-$ [521], $7/2^-$ [514], $5/2^-$ [512] and $9/2^+$ [624] states is in complete agreement with the assignments of de Voigt et al. [40]) deduced from the properties of the rotational bands observed in ^{181}Pt by in-beam experiments. The 235.7 level can be identified as the 9/2 member of the $7/2^-$ [514] rotational band, and the 256.6 and 380.3 keV levels as the 7/2 and 9/2 states of the $5/2^-$ [512] rotational band. The spin and parity values reported for the other states have been obtained using the spin and parity values of the states clearly identified in both the present work and the in-beam experiments [40]), and the transition multipolarities determined in the present work.

Since the 120.6 and 170.5 keV lines are E1, the 287.3 keV level has positive parity. The 534.6, 599.2, 656.3, 678.5, 1158.6, 1198.6, 1798.1 and 1807.8 keV γ-lines are observed in coincidence with both the 170.5 and 159.4 keV γ-rays (see fig. 7a and 7b). This indicates the existence of an unobserved 11.1 keV transition which links the 287.2 keV and 276.2 keV levels. Its total intensity has been evaluated to be 250±150 from the intensity balance of the 287.3 and 276.2 keV levels assuming an E1 multipolarity for the 19.7, 30.6 and 40.5 keV transitions and a total conversion coefficient ∿1 for the 159.4 keV abnormal E1 transition.

It is worth noting that the very intense electron line (noted K 1309.2 Pt + Ir in fig.4a) observed in the electron spectrum with an energy corresponding to a 1309 keV transition converted in the K subshell of platinum, cannot correspond to the E1 1309.2 keV transition in ^{181}Ir (see 3.2.3. and fig.5). It could de-excite the 1309.5 keV state of the ^{181}Pt (see fig.6).

About 92% of the total intensity attributed to the β^+/EC decay of ^{181}Au→^{181}Pt has been accounted for in the level scheme shown in fig.6. 58 levels have been established. The 2085.2 and 2101.8 keV levels are the most populated in the β^+/EC decay of ^{181}Au : their feedings are 12% and 11% respectively. The corresponding transitions (logf_0t = 4.9) are then allowed (ΔJ=0,1 and $\Delta\pi$=+ [ref.[54])] . This indicates that the possible spin and parity values of the ^{181}Au ground state are I^π = 3/2$^-$, 5/2$^-$ or 7/2$^-$.

4. Discussion

4 - 1 ^{177}Ir levels

The levels of ^{177}Ir established from the α decay of ^{181}Au could correspond to states arising from the "h $_{9/2}$ system", for the following reasons :

i) Rotational bands built on the 1/2$^-$[541] ($h_{9/2}$ parentage), 1/2$^+$[660], 5/2$^+$[402] and 9/2$^-$[514] levels have been observed in ^{177}Ir by Dracoulis et al. [55]) from in-beam experiments, but the ground state could not be exactly identified ; it can correspond to the 1/2$^-$[541] or to the 9/2$^-$[514] orbital [55]). From the energy of the Fermi level in the Ir isotopes, and from Au and Ir systematics, the ^{177}Ir ground state is more likely the 5/2 1/2$^-$[541] state.

ii) The parity of the ^{181}Au ground state has been determined to be negative (see 3.2.4). From Au systematics, negative parity states expected to be located at low energy in ^{181}Au come from the "$h_{9/2}$ system" and the most probable ground state of ^{181}Au is then the 5/2 1/2$^-$[541] state.

iii) The approximate hindrance factors F (see fig.3 and 8) for the 5.348, 5.462 and 5.609 MeV α emissions indicate that these α transitions are unhindered. This confirms that the states observed in ^{177}Ir have a structure similar to that of the ^{181}Au ground state, and that they come from the $h_{9/2}$ subshell.

iv) The energy of the observed ^{177}Ir levels added to the F values suggest that the ground state, the 43, 84, 148.4 and 220 keV levels are respectively the $5/2^-$, $9/2^-$, $1/2^-$, $3/2^-$ and $7/2^-$ states of the "$h_{9/2}$ system" (see fig.8). Furthermore the F value found for the α branch to the 267 keV level implies a spin value I=3/2, 5/2 or 7/2 for this state.

4 - 2 ^{181}Ir levels

The negative parity levels established correspond to the low-spin states of the "$h_{9/2}$ system". Their decay mode is similar to that observed for the low-spin negative-parity states previously identified in ^{185}Ir [refs. 56,57)]. Fig.9a shows the large similarity of the negative-parity level schemes of ^{185}Ir and ^{181}Ir. Nevertheless, the second $3/2^-$ level appears at lower energy than the $5/2^-$ level in ^{181}Ir. Such an ordering has been predicted for the neutron-deficient Ir isotopes (see fig.7 of ref. 59) in the framework of a rotor-plus-quasiparticle model assuming axial symmetry 60).

The 289.4, 342.4 and 440.8 keV levels were previously identified as the $3/2^+$[402], $1/2^+$[400] and 3/2 $1/2^+$[400] by Schück et al. 38,39) using Ir systematics. The spin and parity values determined for these states in the present work are in agreement with this identification. Furthermore the 393.6 keV level which decays only towards the 289.4 keV state can be identified as the rotational state 5/2 $3/2^+$[402] and the 569 keV level which de-excites to the 342.4 and 440.8 keV states as the 5/2 $1/2^+$[400]state. Fig.10 shows that the energies of the intraband transitions observed in ^{181}Ir are very similar to those observed for the corresponding transitions in ^{183}Ir and ^{185}Ir. However we note that the 307.0, 413.3 and 542 keV levels of ^{183}Ir have been identified as members of the $5/2^+$[402] rotational band by Janzen et al. 61) from an in-beam experiment. But the rotational band so identified would have a moment of inertia larger than that known in the ^{177,179,181}Re isotopes [51] : the energy of the 7/2 5/2$^+$[402] → 5/2$^+$[402] transition is 105 keV in ^{183}Ir [ref.[61]] and 122, 124 and 118 keV in ^{177}Re, ^{179}Re and ^{181}Re [ref.[51]] respectively. Moreover such a 5/2$^+$[402] would de-excite only towards the 5/2 1/2$^-$[541] state. Therefore the 307.0 and 413.3 keV levels of ^{183}Ir are very likely the 3/2$^+$[402] and 5/2 3/2$^+$[402] states. This implies that the rotational band observed by Janzen et al. [61] is built on a 3/2$^+$ and not on a 5/2$^+$ state. This interpretation coincides with the one proposed in ref.[58]. The 542 keV level then has spin 7/2 but it is located at too low an energy to be the 7/2 3/2$^+$[402] (see fig.10). It could correspond to the 7/2$^+$ built on an unobserved 5/2$^+$[402] state. From the moment of inertia expected for the 5/2$^+$[402] band, the band head would then be expected to lie just above the 413.3 keV level. The wave functions of these two levels would therefore be an admixture of the 5/2$^+$[402] and 5/2 3/2$^+$[402] states.

On the other hand, the 5/2 1/2$^-$[541] state in ^{181}Re decays only via the 356.7 and 238.8 keV transitions towards the 5/2$^+$[402] band and its half life is rather long ($T_{1/2}$ = 96 ns) [ref.[51]]. In ^{181}Ir, if the 289.4 keV level were the 5/2$^+$[402] state, one would expect a long half life, which is not actually the case. This supports also the contention that the 289.4 keV level is the 3/2$^+$[402] and not the 5/2$^+$[402] state.

The level located at 298.9 keV in ^{181}Ir decays to both the 5/2 1/2$^-$[541] and 1/2$^-$[541] states. It has spin and parity values I^π = 3/2$^+$, and its identification is not obvious. A state not easily identified, has also been found at 442.1 keV in ^{185}Ir [ref.[56]] and at 419.1 keV in ^{183}Ir [ref.[38]]. In ^{185}Ir spin and parity values I^π = 5/2$^+$ have been ascribed to this level because of an E2 multipolarity adopted for the 109.8 keV transition whereas the conversion coefficient measured (α_k = 1.3 ± 0.5) [ref.[56]] is also compatible with an E2 + M1 multipolarity. Consequently the 442.1 keV level of ^{185}Ir can also have spin and parity values I^π = 3/2$^+$. The presence of a 3/2$^+$ state at such a low energy, possibly the intruder 3/2$^+$[651] state, would imply a large deformation for the Ir nuclei, which is debatable.

TABLE 4

4-3 ^{181}Pt levels

All the levels of ^{181}Pt located below 280 keV have already been identified (see sec. 3-2-4). The positive-parity level located at 287.3 keV decays to the $7/2^-$[514], $5/2^-$[512], 7/2 $5/2^-$[512] and $9/2^+$[624] states : it is therefore likely the $7/2^+$[633] Nilsson state. Indeed when the neutron number decreases, this state comes close to the Fermi level : it is located at 706.5 keV in ^{185}Pt [ref.[12])] and at 375.0 keV in ^{183}Pt [ref.[16])]. The 650.8 keV level which decays only to the 287.3 keV state could be then the $5/2^+$[642] state.

From N = 103 systematics, the $1/2^-$ [510], $3/2^-$[512], $5/2^-$[523], $3/2^-$[521] and $7/2^-$[503] states are also expected to be present in ^{181}Pt (fig.11). Above 600 keV the level density is very high and no intraband connections appear clearly ; an identification of states is therefore very difficult. However the 525.1, 597.7, 658.9 and 760.5 keV levels which decay only towards the $7/2^-$[514] and $5/2^-$[512] rotational bands could correspond to states belonging to the $5/2^-$[523] and $7/2^-$[503] rotational bands whereas the other states which mainly decay to the $1/2^-$[521] rotational band would belong to the $1/2^-$[510], $3/2^-$[521] and $3/2^-$[512] bands. Thus the 597.7 level which decays only to the $7/2^-$[514] and $5/2^-$[512] states could correspond to the $5/2^-$[523] state whereas the 525.1 keV level which decays also towards the 7/2 $5/2^-$[512] and 9/2 $7/2^-$[514] states could be the $7/2^-$[503] state. In the same way, the 750.4 keV level could correspond to the $1/2^-$[510] state since it decays only towards the 3/2 $1/2^-$[521] state, a decay mode similar to that observed for the $1/2^-$[510] state in ^{183}Os [ref.[12])]. All of these identifications are summarized in fig.12.

It is worth noting that all the experimental levels located below 500 keV could be identified as Nilsson states corresponding to a prolate-shaped nucleus. No shape coexistence seems to be present at low energy in ^{181}Pt. Nevertheless, up to now, the high level density observed between 700 and 1000 keV is still unexplained. Theoretical calculations should be performed to identify more experimental levels and to reach some conclusion on the possibility of shape coexistence. Indeed it would be inte-

541.9 ! 37 ! 1426.6,1436.4

resting to compare theoretical predictions obtained in the framework of a quasiparticle coupled to an axial rotor [60]with our experimental results since such a model has already successfully reproduced the proton states of nuclei in this mass region [59]. This type of calculation is in progress and will be presented in a forthcoming publication. Since dynamical effects seem to be important in platinum isotopes [62] a theoretical calculation performed in the framework of the Bohr-Mottelson unified model, where the quasiparticle and the core are determined by a consistent microscopic description, would have to be used to describe the platinum isotopes. Indeed such an approach, which has already been applied with success in light nuclei [22], would perhaps allow us to understand the high level density.

4-4 Highly-converted transitions

Nine transitions have been found to have high conversion coefficients. One of them, which has been located in the ^{181}Ir level scheme, has a conversion coefficient 4.4 times that of an M1 transition. Therefore, for the first time a highly-converted transition has been identified in an Ir nucleus. This transition (713.7 keV) de-excites the 825.9 keV level towards the $1/2^-$ state located at 112.2 keV. Unfortunately the spin value of the 825.9 keV level can be 1/2 or 3/2 and the nature of the 713.7 keV transition could not be exactly determined ; it is either abnormal M1 or E0 + M1 +E2. The other highly-converted transitions likely occur in ^{181}Pt. The 1309.2 and 583 keV γ-lines correspond to transitions in ^{181}Ir ; however the energies of the observed electron lines do not correspond to conversion of these transitions in Ir but rather to conversion in platinum. The intensities of the Pt γ-lines could not be determined very precisely and only limits have been obtained for the conversion coefficients α_k. The 709.0, 903.5 and 1246.8 keV γ-lines are members of doublets : however from the energy determined for electron lines, it has been possible to assign an electron-line to one of the γ-lines of each doublet and α_k limits could be evaluated.

The ratio R of the experimental α_k value to the theoretical α_k value for an M1 transition is especially large for the 1102.1 keV and 1309.2 transitions (see table 6). For most of these highly-converted transitions the γ-ray intensity is so weak, that they could not be located in the level scheme from coincidence relationships. The 668.5 keV line de-excites the $I^{\pi} = 5/2^{-}$ or $7/2^{-}$ 835.4 keV level to the 166.7 keV $5/2^{-}$[512] state. The 1246.8 keV transition de-excites the most populated $I^{\pi} = 1/2\ 3/2\ 5/2^{-}$ level located at 2101.8 keV to the $I^{\pi} = 3/2\ 5/2\ 7/2^{-}$ 855.0 keV state. The 1309.2 keV transition could de-excite the 1309.5 keV level towards the $1/2^{-}$ ground state. In all these cases it is not possible to define the exact nature of the highly-converted transitions.

We note that the R values (see table 6) for some of the highly-converted transitions observed in ^{181}Pt are as large as those determined in the ^{187}Pt and ^{183}Au isotopes [12] whereas no highly-converted transitions (R>2) were observed in ^{183}Pt [ref.[16]]. A shape transition from oblate or more likely triaxial shape to a prolate shape has been clearly established between ^{187}Pt and ^{185}Pt [ref.[14]]. Therefore, the existence of highly-converted transitions in ^{181}Pt could be the signature for a new shape transition. The moments of inertia observed for the rotational ground-state band of the even platinum isotopes (fig.13) suggest that a shape coexistence at low excitation energy is present in the ^{176,178}Pt isotopes [10]. This supports the contention that a new shape transition occurs in the very neutron-deficient platinum isotopes.

We would like to thank the staff of the Orsay synchrocyclotron for their cooperation during the experiments. We are indebted to the Service Electronique Physique (IPN) who designed and constructed the data acquisition system and to R. Breuil who continuously assisted us. We are grateful to Professor John Crawford for his critical reading of the manuscript. We would also like to thank the S.T.I.C. (IPN) for programming assistance in the data analysis.

1362.5 ! 41 ! 94.0,645.5,(658.4) 1456.5 + 94.0

References

1 - M. Finger et al., Nucl. Phys. A188 (1972) 369.

2 - M. Cailliau, thèse, Orsay (1974).

3 - M.A. Deleplanque et al., J. de Phys. 36 (1975) C5-97.

4 - A. Ben Braham et al., Nucl. Phys. A332 (1979) 397.

5 - J.L. Wood, in Lasers in Nuclear Physics, Nucl. Sc. Res. Conf. series (Harwood, N.Y.1982), p.481.

6 - B.E. Gnade, R.W. Fink and J.L. Wood, Nucl. Phys. A406 (1983) 29.

7 - B. Roussière, C. Bourgeois, P. Kilcher, J. Sauvage, M.G. Porquet, Nucl. Phys. A438 (1985) 93.

8 - B. Roussière, thèse, Orsay (1986).

9 - J.C. Waddington et al., McMaster Accelerator Laboratory, Annual Report (1986) 24.

10 - G.D. Dracoulis et al., J. Phys. G12 (1986) L97.

11 - G. Hebbinghaus et al., Z. Phys. A328 (1987) 387.

12 - B. Roussière, C. Bourgeois, P. Kilcher, J. Sauvage, M.G. Porquet, A. Wojtasiewicz and the ISOCELE Collaboration, Nucl. Phys. A485 (1988) 111.

13 - R. Eder et al., Hyperfine Interactions 43 (1988) 469 and ref. therein.

14 - H.T. Duong et al., Phys. Lett. 217 (1989) 401.

15 - G.D. Dracoulis, B. Fabricius, R.A. Bark, A.E. Stuchbery, D.G. Popescu and T.Kibedi, ANU-P/1041 (1989).

16 - B. Roussière, C. Bourgeois, P. Kilcher, J. Sauvage, M.G. Porquet and the ISOCELE Collaboration, Nucl. Phys. A504 (1989) 511.

17 - Th. Hilberath, St. Becker, G. Bollen, M. Gerber, H.J. Kluge, U. Krönert and G. Passler, Z. Phys. A332 (1989) 107.

18 - K. Kumar and M.Baranger, Nucl. Phys. A110 (1968) 529.

19 - R. Bijker, A.E.L. Dieperink, O. Scholten and R. Spanhoff, Nucl. Phys. A344 (1980) 207.

20 - J. Sauvage-Letessier, P. Quentin and H. Flocard, Nucl. Phys. A370 (1981) 231.

21 - K. Heyde, P. Van Isacker, M. Varoquier, J.L. Wood and R.A. Meyer, Phys. Rep. 102 (1983) 291.

22 - P.Quentin, Proc. 4ème colloque franco-japonais, Seillac (1986) p.83, published by DOC CEN Saclay 87-022.

23 - N. Redon, thèse, Lyon (1987).
24 - R. Bengtsson et al., Phys. Lett. B183 (1987) 1.
25 - L. Bennour, thèse, Orsay (1987).
26 - I. Deloncle, thèse, Orsay (1989).
27 - P. Bonche et al., Nucl. Phys. A500 (1989) 308.
28 - J.K.P. Lee et al., Phys. Rev. C38 (1988) 2985.
29 - J. Bonn, G. Huber, H.J. Kluge, L. Kugler and E.W. Otten, Phys. Lett. B38 (1972) 308.
30 - G. Ulm et al., Z. Phys. A325 (1986) 247.
31 - J.K.P. Lee et al., Proc. 5th Int. Conf. on Nuclei far from Stability, Rosseau Lake (1987), AIP Conf. Proc. n°164 (1988) p.205.
32 - K. Wallmeroth et al., Nucl. Phys. A493 (1989) 224.
33 - J. Nyberg, Thesis, Stockholm (1987) and J. Nyberg et al., Nucl. Phys. A511 (1990) 92.
34 - S. Pilotte, G. Kajrys, S. Monaro and M.P. Carpenter. Phys. Rev. Lett. 40 (1989) 610.
35 - M.C. Abreu, C. Bourgeois, P. Kilcher, M.G. Porquet, B. Roussière, J. Sauvage, Rapport Annuel IPNO-DRE (1987)p.17.
36 - F. Brangança Gil et al., Portgal. Phys. 15 (1984) 59.
37 - E. Hagberg, P.G. Hansen, P.Hornsh0j, B. Jonson, S. Mattsson and P.Tidemand-Petersson, Nucl. Phys. A318 (1979) 29.
38 - C. Schück, V. Berg, A. Zerrouki, J. Genevey-Rivier, A. Knipper and C. Richard-Serre, Rapport d'activité CSNSM, Orsay (1978-1980) 21.
39 - C. Schück, A. Knipper, C. Richard-Serre, V. Berg, A. Zerrouki, J. Genevey-Rivier and the ISOLDE Collaboration, Proceedings of Int. Symp. on Future. Direction on Studies of Nuclei far from Stability, Nashville, Tennessee (1980) 127.
40 - M.J.A. de Voigt et al., Nucl. Phys. A507 (1990) 447.
41 - J.C. Putaux et al., Nucl. Inst. and Meth. 186 (1981) 321.
42 - J. Sauvage et al., Proc. TRIUMF-ISOL Workshop, Mont Gabriel, Québec (1984).
43 - P. Paris et al., Nucl. Instr. and Meth. 186 (1981) 91.
44 - J.T. Routti and S.G. Prussin, Nucl. Instr. 72 (1969) 125.
45 - S.E.T.I., Rapport interne IPNO 87-03 (1987) 42.
46 - J. Van Klinken, S.J. Feenstra and G. Dumont, Nucl. Inst. and Meth. 151 (1978) 433.
47 - R. Turcotte, Ph. D. Thesis 1988 and refs. therein.

48 - H. Dautet, private communication.

49 - R. Gummick and J.B. Niday, Computerized Analysis by γ-ray Spectrometry, UCRL 51061, Vol.1 (1972).

50 - Jagdish K. Tuli, Nuclear Wallet Cards (1985).

51 - C.M. Lederer and V.S. Shirley, Table of Isotopes, 7th ed. (Wiley, New-York, 1978).

52 - C. Bourgeois, P. Kilcher, B. Roussière J. Sauvage, M.G. Porquet, Int. Symp. on In-Beam Nuclear Spectroscopy, Debrecen (1984).

53 - B. Roussière et al., Int. Conf. on Nuclear Shapes, Crête, Grèce (1987), proceedings vol.1, p.79.

54 - S. Raman and N.B. Gove, Phys. Rev. C7 (1973) 1995.

55 - G.D. Dracoulis, B. Fabricius, T. Kibedi, A.E. Stuchbery, ANU-P/1052 (1989) 40.

56 - C. Schück, J. Genevey-Rivier, V. Berg, A. Knipper, G. Walter, C. Richard-Serre and A. Höglund, Nucl. Phys. A325 (1979) 421.

57 - S. André, J. Genevey-Rivier, J. Treherne, R. Kaczarowski, J. Lukasiak, J. Jastrzebski and C. Schück, Nucl. Phys. A325 (1979) 445.

58 - A.J. Kreiner, J. Davidson, M. Davidson, P. Thieberger, and E.K. Warburton, Phys. Rev. in press.

59 - M.G. Porquet, J. Sauvage, M. Meyer, P. Quentin, Nucl. Phys. A451 (1986) 365.

60 - M. Meyer, J. Danière, J. Letessier and P. Quentin, Nucl. Phys. A316 (1979) 93.

61 - V.P. Janzen et al., Phys. Rev. Lett. 61 (1988) 2073.

62 - I. Deloncle, J. Libert, L.Bennour, P. Quentin, Phys. Lett. B233 (1989) 16.

63 - G.D. Dracoulis, C. Fahlander and A.P. Byrne, Nucl. Phys. A401 (1983) 490.

Table captions

Table 1 - Main γ-lines observed in the ^{181}Hg decay and not observed in the ^{181}Au decay.

a) $\Delta E_{\gamma} \lesssim 0.2$ keV

b) $\Delta I_{\gamma} \lesssim 15\%$

c) Part of this γ-line could belong to the β^{+}/EC decay of ^{177}Pt.

Table 2 - α-rays emitted in the decay of ^{181}Au nuclei.

Table 3 - Main γ-lines belonging to the $^{181}Pt \rightarrow {}^{181}Ir$ decay.

1) $\Delta E_{\gamma} \lesssim 0.2$ keV if $I_{\gamma} > 10$ and 0.3 keV in the other cases

2) $\Delta I_{\gamma} \lesssim 15\%$. The intensities have been normalized taking the 112.2 keV γ-intensity as reference ($I_{\gamma} = 100$)

a) γ-ray mixed with a γ-line belonging to the β^{+}/EC decay of ^{181}Au. The intensity has been evaluated from coincidence spectra

b) doublet

Table 4 - γ-ray data for the $^{181}Au \rightarrow {}^{181}Pt$ decay

a) $\Delta E_{\gamma} \sim 0.1$ keV if $I_{\gamma} > 20$ for $E_{\gamma} < 500$ keV and $I_{\gamma} > 50$ for $E_{\gamma} > 500$ keV

$\Delta E_{\gamma} \lesssim 0.3$ keV for the other cases

b) $\Delta I_{\gamma} \sim 15\%$. The 170.5 keV γ-intensity has been taken as reference ($I_{\gamma} = 100$)

c) γ-line not clearly assigned to the $^{181}Au \rightarrow {}^{181}Pt$ decay

* γ-line mixed with a γ-ray attributed to the $^{181}Pt \rightarrow {}^{181}Ir$ decay. The intensity has been estimated from coincidence spectra.

** doublet.

Table 5 - Electron data for the decay of ^{181}Au . For the mixed electron lines global intensity is reported.

- * the electron line corresponds to a transition of 1309.6 keV in Pt whereas the 1309.2 keV γ-ray can be clearly attributed to the Ir from coincidence relationships.
- ** doublet
- a) The L709 keV contribution has been subtracted

Table 6 - Highly-converted transitions in ^{181}Pt and ^{181}Ir

Figure Captions

Fig. 1a Schematic view of the electron detection system.

1b Efficiency curve of the electron detection.
o ^{188}Pt decay, Δ ^{188}Ir decay

Fig. 2 Decay chain of ^{181}Hg. Data have been taken from ref.[50].

Fig. 3 α decay scheme of ^{181}Au. F is the hindrance factor determined according to ref.[51]. The energies of ^{177}Ir levels are given in keV.

Fig. 4a Conversion-electron and γ-ray spectra recorded in the ^{181}Au decay (low-energy part). Energies are reported in keV. Electron lines are marked by their corresponding γ-ray energy and the converting electron shell. Lines belonging to the $^{181}Pt \rightarrow ^{181}Ir$ decay are marked by Ir.

Fig. 4b Conversion-electron and γ-ray spectra recorded in the ^{181}Au decay (high-energy part). (See fig.4a caption).

Fig. 5 Partial level scheme of ^{181}Ir. The transitions not observed in coincidence are drawn in dashed lines.
* indicates ray mixed with ^{181}Pt ray.
** indicates doublet.

Fig. 6 Level scheme of ^{181}Pt. The transitions which could not be observed in coincidence either because of their weak intensity or their location with respect to the 116.8 keV isomeric or the ground state, are shown as dashed-lines. Spin values eliminated by dashed-line transitions are indicated in parentheses.
* transitions placed twice in the level scheme.
** doublet.

Fig. 7a Coincidence spectra for gates set on the 198.6, the 170.5 and the 159.4 keV γ-lines (low-energy part). Energies are in keV. B.S. indicates lines generated by back scattering.

Fig. 7b Same as fig. 7a for high-energy part.

Fig. 8 Systematics of low-spin states arising from the h9/2 subshell in light Ir isotopes. F is the hindrance factor (see fig.3 caption).

Fig. 9 Negative-parity states corresponding to the "h 9/2 sys tem" in ^{181}Ir and ^{185}Ir. ^{185}Ir data have been taken from refs.[56,57] and the 13/2, 17/2 and 21/2 levels of ^{181}Ir from ref.[58]. Spin values have been multiplied by 2.

Fig. 10 Systematics of positive-parity levels. States of the 1/2^{+}[400] rotational band are indicated by —, those of the 3/2^{+}[402] by -X-. ^{185}Ir data have been taken from ref.[56] and ^{183}Ir data from refs.[38,39,61]. The 542 keV level in ^{183}Ir is discussed in sec. 4-2.

Fig. 11 Systematics of the intrinsic states through the N=103 isotones. Data have taken from refs.[51,63].

Fig. 12 Experimental levels of ^{181}Pt arranged in quasi-rotational bands. Arrows represent one or several transitions towards states indicated by arrowheads. Spin values are multiplied by 2. The remaining experimental levels are shown up to 1 MeV on the right of the figure.

Fig. 13 Kinematical moment of inertia, $\mathcal{J}^{(1)}$, versus angular velocity, ħω, for the even-A platinum isotopes.

TABLE 1

E_γ(keV)[a)]	I_γ[b)]
30.8	13
42.5	76
147.8[c)]	300
157.4	16
165.8	16
180.1	≈16
185.0	≈33
194.7	10
210.9	19
214.1	≈13
217.9	7.3
223.2	32
265.4	29
281.0	11
330.9	21
385.6	18
1202.2	15
1394.4	18
1776.9	27
1986.7	50

the 5/2 $1/2^-[541]$ state.

TABLE 2

This work		Previous work [ref.[37])]	
E_α (MeV)	$I_\alpha$rel (%)	E_α (MeV)	$I_\alpha$rel (%)
5.348 ± 0.006	4.8 ± 0.2	5.365 ± 0.010	6 ± 1
5.393 ± 0.008	1.5 ± 0.2		
5.462 ± 0.004	46.5 ± 1.1	5.480 ± 0.008	44 ± 10
5.527 ± 0.008	1.5 ± 0.2		
5.567 ± 0.012	1.3 ± 0.2		
5.609 ± 0.008	44.4 ± 1.1	5.625 ± 0.005	50 ± 9

TABLE 3

E_γ (KEV)[1]	I_γ[2]	MAIN COINCIDENT γ-RAYS	LOCATION
24.9			
98.6	4.0	112.2,230.2,1309.2	440.8→342.4
98.9	≈2.5		(342.4→243.2)
104.2	≈2	289.4	393.6→289.4
112.2	100	98,131.3,186.8,198.6,230.2,335.6,348.3,370.7,402.7,479.2, 489.8,524.2,533,638.1,(733.5),905.7,917.7,960.6,1021.7, 1309.2,1407.8,1555.7,1568.8,1587.0,1638.1	112.2→0
128.3	3.8	(98),230.2	(569.0→440.8)
131.3	16	112.2,249.1,348.3,402.7,(582.7),(586.4),905.7,960.6	243.2→112.2
144	≈2	335.6	591.3→447.7
182.1	1.4	285.3,310.2	492.3→310.2
186.8	5.6	480.9,533	298.9→112.2
198.6a)	≈9	112.2,335.6,447.5,905.7	646.0→447.7
204.6	1.0	131.3,243.2	447.7→243.2
226.6	≈2.1		(569.0→342.4)
230.2	92	98,112.2,128.3,226.6,480.9,489.8,638.1,539.5,769.7,773.5, 917.7,1213.1,1309.2,1407.8	342.4→112.2
243.2	61	249.1,348.3,402.7,524.2,582.7,586.4,(722.2),(869.1),905.7 960.6,(1059.5)	243.2→0
249.1	4.6	(112.2),131.3,243.2,1059.5	492.3→243.2
285.3	5.4	182.1,519.3,(722.2)	310.2→24.9
289.4a)	100	104.2,(533),917.7	289.4→0
298.9	12	(112.2),533,917.7,1368.6	298.9→0
310.2	8.5	519.3,722.2,869.1	310.2→0
335.6	28	112.2,198.6,905.7	447.7→112.2
341.6	3.7		
348.3	24	112.2,131.3,243.2,960.6,(1076.5),1159	591.3→243.2
370.7	4.9	112.2,(198.6),(243.2),402.7,533,733.5	(1016.7→646.0)
402.7a)	≈18	112.2,131.3,243.2,370.7,905.7,1053.0	646.0→243.2
440.5	7.0	1309.2	(440.8→0)
447.5	13	198.6,905.7	447.7→0
479.2	26	112.2,960.6,1108,(1159)	591.3→112.2
480.9a)	≲10	230.2,(335.6)	
489.8	7.5	112.2,230.2,917.7	832.2→342.4
492.0a)	≲10		(492.3→0)
519.3	4.5	285.3,310.2,722.2	829.6→310.2
524.2a)	12	112.2,243.2,335.6	
533.2	24	112.2,186.8,298.9,370.7,733.5,905.7,917.7,1021.7,1053.0,	832.2→298.9
533.8	36	1128.3	646.0→112.2
539.5	≈4	98,230.2,769.7	980.5→440.8
543	≈3	289.4,917.7	832.2→289.4
568.8	6.5	(131.3),(335.6)	(1016.7→447.7)
582.7	8.6	112.2,131.3,243.2	825.9→243.2
586.4	4.2	131.3,243.2,722.2	829.6→243.2
591.0a)	24	(112.2),480,960.6,1108	591.3→0
621.9	4.0		
638.1	5.8	112.2,230.2,769.7	980.5→342.4
691	5.8		(980.5→289.0)
713.7	4.6	112.2	825.9→112.2
722.2	5.6	131.3,243.2,285.3,310.2,519.3,586.4	1551.8→829.6
733.5	13	112.2,(243.2),(285.3),(335.6),370.7,402.7,479.2,(533)	(1750.1→1016.7)
738.8	8.9	(335.6)	
769.7	11	112.2,230.2,539.5,638.1,691	1750.1→980.5
773.5	≲5	112.2,230.3,(691)	
828.8	2.8	131.3,(243.2)	
869.1	9.6	(243.2),285.3,310.2,586.4	1699.0→829.6
905.7	42	112.2,131.3,198.6,243.2,335.6,402.7,447.5,533	1551.8→646.0
917.7	19	112.2,230.2,289.4,298.9,489.8,533,543	1750.1→832.2
960.6	29	112.2,131.3,(144),170.5,243.2,335.6,348.3,479.2,591.0	1551.8→591.3
1021.7	7.5	112.2,198.6,(230.2),(335.6),402.7,533	1667.8→646.0
1053.0	9.5	112.2,243.2,(335.6),402.7,480,533	1699.0→646.0
1059.5	5.3	243.2,249.1,310.2,480,492.0	1551.8→492.3
1076.5	≲8.6	112.2,348.3,479.2,591.0	1667.8→591.3
1079.5	3.4	(230.2)	
1104.3	4.0	112.2,335.6	1551.8→447.7
1108	≈5	243.2,348.3,479.2,591.0	1699.0→591.3
1128.3a)	≈5	112.2,(198.6),402.7,533	[illegible]→646.0
1159 a)	≈9	348.3,479.2,(591.0)	1750.1→591.3
1213.1	6.3	112.2,230.2	1555.5→342.4
1302.6	3.9	112.2,(204.6),335.6,(447.5)	1750.1→447.7
1309.2a)	≲28	98,112.2,230.2,(440.5)	1750.1→440.8
1338.7	5.1	112.2,230.2	1680.9→342.4
1354.7	5.0	(112.2)	
1368.6	4.8	(298.9)	1667.8→298.9
1407.8	22	112.2,230.2	1750.1→342.4
1507	2.1	(243.2)	(1750.1→243.2)
1555.7	5.4		1667.8→112.2
1568.8	5.5		(1680.9→112.2)
1587.0	24	112.2	1699.0→112.2
1638.1	10	112.2	1750.1→112.2
1668.2b)	≲12	(112.2)	(1667.8→0)
1680.7	12		(1680.9→0)
1698.9	18		(1699.0→0)

TABLE 4

E_{γ} [a] (keV)	I_{γ} [b]	Main coincident γ-rays	Location
11.1			287.3 → 276.2
14.5			94.0 → 79.4
19.7	15±5	89.9	276.2 → 256.6
22.8	23±8	94.0	116.8 → 94.0
30.6	1.7		287.3 → 256.6
40.5	67	79.4,94.0,118.9,(545.9),610.4,(644.4)	276.2 → 235.7
50.0	92	89.9,(94.0),120.6,123.8,(213.6),358.4,402.6,431.0,491.9,(668.5),688.7 (749.8),751.0,920.5,(1935.9),1960.0,1970.6	166.7 → 116.8
72.6	∿ 50	(89.9),94.0,120.6,431.0	166.7 → 94.0
79.4	∿250	87.3,184.3,198.6,206.9,603.3,614.7,629.2,650.0,671.0,704.4,775.5, 789.2,792.2,809.4,823.8,825.4,(960.5),962.7,1048.6,1230.0, 1393.1,1935.9,(1973.8),1991.1,2001.2,2005.6,2022,4,2043.1,2058.1	79.4 → 0
87.3	28	79.4,89.9,120.6,123.8,(213.6),358.4,431.0,688.7,(749.8),751.0,(920.5) (960.5),(962.7),(1089.2),(1970.6)	166.7 → 79.4
89.9	44	19.7,50.0,87.3,94.0,123.8,402.7,(624.9),749.8,999.7,1183.6	256.6 → 166.7
94.0	220	22.8,(50.0),72.6,(120.6),162.6,184.3,206.9,(431.0),614.7,(645.5), 671.0,709.8,741.4,756.4,787.4,(843.8),995.0,1215.5,1362.5,1393.1, (1417.7),1991.1,2001.2,(2032.6)	94.0 → 0
118.9	68	40.5,144.6,(289.4),423.2,525.5,610.4,656.3,774.6,(785),808.7,1032.4, 1034.8,1158.5,1198.6	235.7 → 116.8
120.6	130	50.0,72.6,(79.4),87.3,(94.0),338.3,363.9,534.6,599.2,633.2,656.3, 678.5,763.3,820.2,845,(886.3),909.1,(960.5),(962.7),1129.4,1158.6, (1163.0),1198.6,1208.4,1798.1,1807.8	287.3 → 166.7
123.8	12	89.9,(380.2)	380.3 → 256.6
132.1	∿ 9	(c)	
139.9	∿ 6	(19.7),(123.8)	(256.6 → 116.8)
144.6	∿ 5	118.9,(380.2)	380.3 → 235.7
159.4	140	534.6,545.9,599.2,610.4,644.4,656.3,678.5,774.6,1158.6,1198.6,1208.4, 1798.1,1807.8	276.2 → 116.8
162.6	6.4	(123.8)	(256.6 → 94.0)
170.5	100	(363.9),452.1,(460.0),534.6,599.2,633.2,656.3,678.5,763.3,820.2, (960.5),(962.7),1129.4,1158.6,(1163.0),1198.6,1798.1,1807.8	287.3 → 116.8
180.3	2.2	(c)	
184.3	37	94.0,557.2,572.6,591.0,603.3,625.7,643.6,688.7,775.5,794.9,(809.4), 1775.0,1804.8,1807,1816.9	278.2 → 94.0
198.6	260*	79.4,294.8,(486.8),(505),557.2,572.6,591.0,603.3,625.7,643.6,688.7, 728.7,775.5,794.9,809.4,(823.8),(1013.1),1048.6,1266.5,1271.2,1775.0, 1804.8,1807,1816.9,1869.0,1875.1	278.2 → 79.4
206.9	65	94.0,482.7,534.6,549.6,579.9,603.3,(621),(666.1),789.2,(904.9), (1007.8),1784,1794.3,1852.6	300.9 → 94.0
213.6	∿ 7	{50.0, 87.3 {358.4	(380.3 → 166.7)
246.4	3.0	610.4 (c)	
255	∿ 4	(c)	
259.2	∿ 3.8	(c)	
263.4	13	380.2	380.3 → 116.8
268.8	9		(525.1 → 256.6)
289.4	∿10*	118.9	525.1 → 235.7
294.8	≲ 10	79.4,198.6	
311.	weak	358.4 (c)	
318.6	4.0		
320.0	2.4	(431.0),(480.9)	(917.7 → 597.7)
338.3	8.6	120.6,656.3,820.2	1281.9 → 943.6
352.4	3.5	(c)	
353.9	2.1	120.6,656.3	
358.4	35	50.0,(87.3),213.6,311,629.2	525.1 → 166.7
363.5	9.2	120.6,(170.5),400.0	650.8 → 287.3
378.2	3.6	(c)	
380.2	9.7	(50.0),(89.9),123.8,263.4	760.5 → 380.3
400.0	6.6	(120.6),363.5,524.2,(1034.8) (c)	1050.7 → 650.8
402.6	∿ 30*	50.0,(87.3),89.9,1426.6,1436.4	658.9 → 256.6
407.3	4.2	(c)	
408.2	24		(525.1 → 116.8)
410.4	9.2	(c)	
412.8	3.5	(c)	
420.1	3.5	(c)	
422.2	3.7	(c)	
423.2	21	118.9,785	658.9 → 235.7
431.0	100	50.0,87.3,650.0,1484.9,1504.4	597.7 → 166.7
435.0	2.9	(c)	
439.7	∿ 10	120.6,661.8,999.7,(1205.4)	
450.5	4.3	(c)	
452.1	5.3	120.6,(159.4),170.5,678,5,684.0	1417.3 → 965.8
455.6	2.8	(89.9),123.8	835.4 → 380.3
460.0	4.5	(50.0),120.6,170.5,534.6,545.9,820.2	1281.9 → 822.0
480.9	∿ 120**	(94.0),(358.4),(408.2),617.7,650.0,(679.9),728.5,775.5,1484.9,1504.4	597.7 → 116.8
482.7	5.1	(94.0),206.9	783.7 → 300.9
486.8	1.9	(79.4),198.6	765.0 → 278.2
491.9	∿ 22*	50.0,(87.3),(1426.6)	658.9 → 166.7
495.8	6.5	(c)	
499.9	3.8	(c)	
504.0	∿ 6	(89.9)	(760.5 → 256.6)
505	∿ 8	198.6	783.7 → 278.2
522.9	4.3		
524.1)	∿25*	400.0,(926.8),982.6 (c)	
525.5	∿ 10	118.9,(785),(792.2)	760.5 → 235.7
527.8	4.7	(c)	
531	weak	120.6,(170.5),(627.5),656.3	1474.3 → 943.6
534.6*	∿ 50**	(50.0),(118.9),120.6,159.4,170.5,206.9,460.0,(595.9),1263,1273	{ 822.0 → 287.3 { (835.4 → 300.9)

541.9	37	1426.6,1436.4	[illegible]
543.	< 10	661.7,775,5,(783.7) (c)	1326.5 → 783.7
545.9	28	40.5,118.9,159.4,460.0,1263,1373	822.0 → 276.2
547.6	4.4	650.0 (c)	
549.6	11	206.9,255,(1245.0)	850.5 → 300.9
552.3	2.4	(c)	
555.5	15	661.7,884.7	
557.2	15	184.3,198.6,(1266.5)	835.4 → 278.2
558.7	4.2	(491.9) (c)	
563.0	4.5	(50.0),(1372.1)	(729.5 → 166.7)
567.3	4.3	(206.9)	(869.2 → 300.9)
572.6	6.3	198.6	850.5 → 278.2
574.9	16	255 (c)	
576.1	10	(c)	
577.2	9.4	(c)	
578.7	10	(50.0),(89.9)	(835.4 → 256.6)
579.9	7.3	206.9	881.4 → 300.9
583	<10		
584.0	4.9	(c)	
591.0	~ 15 *	184.3,198.6	869.2 → 278.2
595.9	13	534.6,545.9,684.0	(1417.9 → 822.0)
597.0	~ 10	650.0,729.6,775.5	1326.5 → 729.5
599.2	19	120.6,159.4,170.5,1198.6,1208.4	886.6 → 287.3
603.3	24	184.3,198.6	881.4 → 278.2
	5	(206.9)	903.8 → 300.9
609.0	5.1		
610.4	48	40.5,118.9,159.4,1198.6,1208.4	886.6 → 276.2
613.8	5.0	(c)	
614.7	36	94.0,1393.1,1417.7	708.7 → 94.0
617.4	10	(431.0),480.9	
621.0	~ 8 *	206.9	921.8 → 300.9
624.9	9.0	(50.0),(89.9)	(881.4 → 256.6)
625.7	11	(184.3),198.6	903.8 → 278.2
627.5	16	(294.8),(531),1474.3	2101.8 →1474.3
629.2	79 **	1393.1,1417.7	708.7 → 79.4
		358.4,(378.2),(408.2)	
633.2	14	120.6,159.4,170.5,1163.0	920.5 → 287.3
635.4	21	(642.2)	729.5 → 94.0
642.2	~ 6.4	635.4,650.0,729.6	1371.7 → 729.5
643.6	27	184.3,198.6,1160.8	921.8 → 278.2
644.4	26	(118.9),(159.4),1163.0	920.5 → 276.2
645.5	33	(94.0),1362.5,1455.7	2101.8 → 1456.5
650.0	110 **	79.4,597.0,642.2,1352.8,1372.1	729.5 → 79.4
		431.0,480.9	
656.3	70	50.0,(87.3),118.9,120.6,159.4,170.5,338.3,(353.9),(531),820.2,1158.5	943.6 → 287.3
658.4	~ 30	(1362.5)	
661.7	160	439.7,884.7,1422.5,1432.9,1439.5,(1474.3),	
		1579.3	
666.1	35	94.0,206.9,(1334.8)	
668.5	23	50.0,(87.3)	835.4 → 166.7
671.0	190 **	79.4,94.0,(1387.3)	765.0 → 94.0
			750.4 → 79.4
677.5	8.6	(c)	
678.5	58	120.6,159.4,170.5,452.1,684.0,1117,1119,1129.4	965.8 → 287.3
679.9	5.5	(431.0),(480.9)	
684.0	25	452.1,(595.9),678.5,(1417.7)	2101.8 →1417.5
685.0	18	(1318.0),(1387.3)	
688.7	~ 40	50.0,(87.3),1246.8	855.0 → 166.2
	~ 20	(94.0),184.3,198.6	966.9 → 278.2
700.9	18	1321.1,1400.6	2101.8 →1400.6
704.4	20	79.4,1318.0	783.7 → 79.4
709.0	8.4	94.0,661.7,729.6,(751.0),1323.5	
709.8	29		
724.3	36	(1318.0),1323.5	
728.7	~ 12	184.3,198.6	1006.4 → 278.2
	~ 12	431.0,480.9,775.5	1326.5 → 597.7
729.6	49	642.2,(661.7),(709.0,709.8),(775.5),(1292.5),1352.8	729.5 → 0
741.4	20	94.0,1266.5	835.4 → 94.0
749.8	20±5	(89.9),	1006.4 → 256.6
751.0	45	50.0,87.3,(709.8),1183.6	917.7 → 166.7
756.4	29	(79.4),94.0,1234.7,1245.0	850.5 → 94.0
763.3	10	(50.0),120.6,(159.4),170.5,1034.8	1050.7 → 287.3
764.5	7.0	(c)	(881.4 → 116.8)
769.0	10	(c)	
772.2	7.4	(c)	
774.6	35	(118.9),159.4,(1032.4),1034.8	1050.7 → 276.2
775.5	40	79.4,(89.9),94.0,184.3.198.6,431.0,480.9,[illegible],597.0,650.0,(728.7,	855.0 → 79.4
	30	729,6),783.7,1048.6,1070.1,1232.7,1246.8,1325.7	2101.8 →1326.5
782.6	41	(c)	
783.7	48	543,775.5,(1064.8),1311,1318	783.7 → 0
785		118.9	
787.4	15	94.0	881.4 → 94.0
789.2	34	206.9,1252.5	
792.2	39	79.4,94.0,(525.5),(962.7),(1007.8),1215.5,1230.0	2101.8 →1309.5
794.9	11	(184.3),198.6	
801.5	10		
808.7	19	118.9,1126.8	
809.4	11	79.4,94.0,184.3,198.6	1087.2 → 278.2
812.7	8	(c)	
820.2	14	(50.0),120.6,159.4,170.5,338.3,460.0,534.7,545.9,656.3	2101.8 →1281.9
823.8	3.4	(c)	
825.4	12	79.4	903.8 → 79.4
834.9	10	(c)	
838.7	7.0	(c)	

841.7	15	(c)	
843.8	21	(94.0) (c)	
845	weak	120.6,159.4,170.5	
846.8	16	(c)	
854.6	~ 11	(120.6),(170.5)	
858.4	5.4	(c)	(1456.5 → 597.7)
868.4	18 *	1225.8	
875.3	6.7		
883.3	~ 6	(c)	
884.7	~ 11	555.5,661.7,1121	
886.3	~ 9	(120.6),(170.5) (c)	
903.5	13	(c)	
904.9	13 *	(206.9),(1064.8) (c)	
909.1	8.1*	120.6,170.5 (c)	
920.5	36	50.0,87.3,(94.0)	1087.2 → 166.7
926.8	15	120.6,(170.5)	
928.5	19		
960.5	≲ 15 *	170.5 (c)	
962.7	35	50.0,87.3,120.6,170.5,1022.4	
969.5	9.0	(c)	
970.8	8.1	(c)	(1087.2 → 116.8)
995.0	~ 9	94.0 (c)	
999.7	33	89.9,(439.7)	1256.3 → 256.6
1007.8	65**		
1013.1	6.1	(79.4),198.6	
1015.5	9.3	809.4,920.4	
1022.4	23	(962.7)	
1032.4	8.6	120.6,170.5,(763.3),(774.6)	2082.7 →1050.7
1034.8	28	(50.0),120.6,159.4,170.5,(363.5),(400.0),763.3,774.6	2085.2 →1050.7
1044.7	3.8	774.6	2095.2 →1050.7
1048.6	16	184.3,198.6,775.5	1326.5 → 278.2
1050.8	9.4		
1062.6	9.6	(c)	
1064.8	9.1	783.7,904.9 (c)	
1070.1	9.4	775.5	(1326.5 → 256.6)
1086.6	20	688.7	2053.0 → 966.9
1089.2	17		(1256.3 → 166.7)
1094.0	19	358.4,480.9,491.9,671.0,1007.8	
1112.6	13		
1117		120.6,170.5,678.5	2082.7 → 965.8
1119	~ 19	120.6,170.5,678.5	2085.2 → 965.8
1121 *		884.7	
1126.8	~ 22	808.7	
129.4	~ 13	120.6,159.4,170.5,678.5	2095.2 → 965.8
1135.7	5.0	(c)	
139.0	5.7	(c)	
141.0	9.1	(c)	
158.5	~ 28 *	120.6,159.4,170.5,656.3	2101.8 → 943.6
160.8	11	643.6	2082.7 → 921.8
163.0	7.8	120.6,159.4,170.5,633.2,644.4	2082.7 → 920.5
164.8	11	(c)	
172.8	7.6	(206.9) (c)	
174.1	6.8	(c)	
176.6	2.5	(c)	
181.3	3.5		
183.6	13	89.9,751.0	
188.8	7.2	(c)	
196.4	4.7	(c)	
198.6	40	120.6,159.4,170.5,599.2,610.4	2085.2 → 886.6
205.4	6.5		
208.4	12	120.6,159.4,170.5,599.2,610.4	2095.2 → 886.6
215.5	47	94.0,792.2	1309.5 → 94.0
225.8	9.3	868.4 (c)	
230.0	24	79.4,792.2	1309.5 → 79.4
232.7	14	94.0,120.6,170.5,775.5,789.2,868.4	(1326.5 → 94.0)
234.7	10	(94.0),756.4	2085.2 → 850.5
245.0	13	756.4	2095.2 → 850.5
246.8	30	688.7,775.5	2101.8 → 855.0
250.3	12	(79.4) (c)	
252.5	23	(783.7),789.2 (c)	
259.4	5.6	(557.2),(578.7) (c)	(2095.2→ 835.4)
263	weak	120.6,159.4,170.5,534.7,545.9	2085.2 → 822.0
266.5	7.0	79.4,198.6,557.2,(578.7),(668.5),741.4	2101.8 → 835.4
271.2	9.6	(198.6)	
273	weak	(120.6),534.7,545.9	2095.2 → 822.0
274.8	6.3	(783.7),825.4 (c)	
278.5	6.7	(c)	
285.4	5.3	(c)	
288.1	9.5	(671.0)	(2053.0 → 765.0)
290.5	weak	(671.0) (c)	
292.5	17	729.6,(809.4) (c)	
297.2	7.7	(c)	
311.1	~ 7*	783.7 (c)	2095.2 → 783.7
309.2	<<10*	(439.7),480.9,(661.8)	
318.0	35	(505),(671.0),685.0,704.4,(724.3),783.7	2101.8 → 783.7
321.1	11	700.9	1400.6 → 79.4
323.5	18	709,724.3	
325.8	22	775.5	1326.5 → 0
332.2	10	671.0	2082.7 → 750.4
334.8	6.2	94.0,666.1	
342.5	8.0	(c)	
348.4	5.2	(c)	
352.8	16	94.0,635.4,650.0,729.6	2082.7 → 729.5
356.8	8.7		(2015.3 → 658.9)

1362.5	41	94.0,645.5,(658.4)	1456.5 → 94.0
1368.6	9.7	(783.7)	(2153.2 → 783.7)
1372.1	47 **	94.0,(486.8),635.4,650.0,(671.0),729.6	2101.8 → 729.5
			(2137.3 → 765.0)
1387.3	10	671.0	2137.3 → 750.4
1393.1	43	79.4,94.0,614.7,629.2	2101.8 → 708.7
1400.6	19	700.9	1400.6 → 0
1417.7	22 **	79.4,94.0,614.7,629.2,(684.0)	2126.5 → 708.7
			(1417.9 → 0)
1422.5	6.7	661.7	
1424.6	12	(671.0)	
1426.6	20	(118.9),402.6,423.2,491.9,541.9	2085.2 → 658.9
1432.9	6.7	(120.6),661.7	
1436.4	22	402.6,(423.2),(491.9),541.9	2095.2 → 658.9
1439.5	21	661.7	
1455.7	17 **	645.5	1456.5 → 0
1459.4	5.5	(c)	
1472.0	6.0	(c)	
1474.4	15	627.5,(661.7)	1474.3 → 0
1484.9	23	431.0,480.9	2082.7 → 597.7
1488.3	12	(c)	
1494.3	6.5	(c)	
1504.4	19	(120.6),(159.4),(170.5),431.0,480.9	2101.8 → 597.7
1511.5	9.8	120.6,170.5	
1530.6	9.9	(c)	
1539.5	5.3	(c)	
1541.8	6.6	(c)	
1551.6	12	(c)	
1576.0	7.6	(c)	
1579.3	9.1	661.8	
1612.5	5.1	(c)	
1615.8	~ 5.0	(c)	
1629.8	8.1	(c)	
1643.7	6.2	(c)	
1705.1	5.2		(2085.2 → 380.3)
1718.1	6.6	(c)	
1730	≲ 4	(c)	
1741.3	12	(c)	
1748.3	6.4	(c)	
1775.0	18	184.3,198.6	2053.0 → 278.2
1779.8	23		
1784	~ 4		2085.2 → 300.9
1785.8	~ 5.0	(c)	
1794.3	16	206.9	2095.2 → 300.9
1798.1	99	120.6,159.4,170.5	2085.2 → 287.3
1804.8	24	184.3,198.6	2082.7 → 278.2
1807	~ 30	184.3,198.6	2085.2 → 278.2
1807.8	~100	120.6,159.4,170.5	2095.2 → 287.3
1816.9	24	79.4,184.3,198.6	2095.2 → 278.2
1829.5	9.2	(c)	
1852.6	7.9	94.0,206.9	2153.2 → 300.9
1860.2	22	(118.9)	(2095.2 → 235.7)
1869.0	6.9	(c)	
1875.1	12	(c)	(2153.2 → 278.2)
1886.2	12	(c)	(2053.0 → 166.7)
1891.2	14	(c)	
1896.3	5.4	(c)	
1917.1	18	(c)	
1920.9	10		(2015.3 → 94.0)
1928.5	14		(2095.2 → 166.7)
1935.9	62 **	(50.0)	2101.8 → 166.7
			2015.3 → 79.4
1941.9	10		
1950.8	9.6		
1960.0	110	50.0,(87.3)	2126.5 → 166.7
1965.9	210		(2082.7 → 116.8)
1968.4	120		(2085.2 → 116.8)
1970.6	66	50.0,87.3	2137.3 → 166.7
1973.8	32	(79.4)	2053.0 → 79.4
1982.5	76	(c)	
1991.1	140	79.4,94.0	2085.2 → 94.0
1996.2	~ 15	(c)	
2001.2	83	94.0	2095.2 → 94.0
2005.6	180	79.4,(198.6)	2085.2 → 79.4
2012.9	~ 8	(c)	
2015.4	86	(198.6)	2015.3 → 0
2022.4	250	79.4	2101.8 → 79.4
2028.3	23		(2122.5 → 94.0)
2032.6	25		(2126.5 → 94.0)
2036.0	49		(2153.2 → 116.8)
2043.1	100		2122.5 → 79.4
2052.6	21		(2053.0 → 0
2058.1	52	79.4	2137.3 → 79.4
2067.0	7.0	(c)	
2072.7	33		
2073.5	23	(79.4)	(2153.7 → 79.4)
2101.8	56		(2101.8 → 0)
2106.8	19	(c)	
2117.7	17	(79.4)	
2126.5	110		(2126.5 → 0)
2136.7	12		(2137.3 → 0)
2140.2	6.2	(c)	
2146.4	16	(c)	

p.83, published by DOC CEN Saclay 87-022.

TABLE 5

E_γ(keV)	Nucleus	Subshell	α	Multipolarity
94.0	Pt	M	1.1±0.2	E2
		N	0.2±0.1	
112.2	Ir	L	1.7±0.6	E2
118.9	Pt	L1+L2	1.15±0.15	M1+E2
120.6	Pt	L	<0.33	E1
148.4	Ir(A=177)	L	0.43±0.15	M1(+E2)
159.4	Pt	L	$\sim$0.04	abnormal E1
170.5	Pt	K	<0.11	E1
184.3	Pt	L	0.13±0.06	M1+E2
198.6	Pt	K	0.16±0.04	E2
	Pt+Ir	L	0.16±0.03	E2
206.9	Pt	K	0.17±0.04	E2
	Pt	M	0.022±0.010	
230.2	Ir	K		E1
243.2	Ir	K	0.33±0.10	M1+E2
		L	0.06±0.02	
268.8	Pt	K	0.63±0.30	M1
		L	0.08±0.04	
285.3	Ir	K	0.23±0.10	M1(+E2)
289.4	Ir	K	0.022±0.010	E1
298.9	Ir	K	0.023±0.010	E1
335.6	Ir	K		M1
			0.18±0.04	
338.3	Pt	K		(M1)
348.3	Ir	K	0.19±0.06	M1
358.4	Pt	K	0.13±0.04	M1+E2
363.5	Pt	K	0.16±0.08	M1
380.2	Pt	K	0.15±0.08	M1
402.7	Ir	L		M1
			0.024±0.007	
402.6	Pt	L		M1
431.0	Pt	K	0.07±0.02	M1+E2
439.7	Pt	K	$\sim$0.07	(M1+E2)
447.7	Ir	K	0.08±0.03	M1+E2
533.2	Ir	K		
533.8	Ir	K	0.038±0.008	
534.6	Pt	K		
539.5	Ir	K		
			0.02±0.01	
541.9	Pt	K		E2(+M1)
549.6	Pt	K	$\sim$0.02	(M1+E2)
582.7	Ir	K	0.025±0.008	M1+E2
583	Pt	K	$\geq$0.20	>M1
591.0	Ir	K	0.034±0.020	M1,E2
603.3**	Pt	K	0.030±0.010	M1+E2
610.4	Pt	K	0.034±0.009	M1(+E2)
614.7	Pt	K	$\sim$0.011	(E2)
629.2**	Pt	K	0.028±0.010	M1(+E2)
643.6	Pt	K		
644.4	Pt	K	0.018±0.006	
645.5	Pt	K		
650.0**	Pt	K	0.020±0.006	M1+E2
656.3	Pt	K	0.009±0.003	E2(+M1)
661.7	Pt	K	$\lesssim$0.024±0.006	E2(+M1)
668.5	Pt	K	0.11 ± 0.04	>M1
671.0**	Pt	K	0.023±0.010	M1+E2
678.5	Pt	K	0.020±0.009	M1+E2
688.7**	Pt	K	0.024±0.010	M1(+E2)

709.0	Pt	K		>M1
			0.13±0.03	
709.8	Pt	K		
713.7	Ir	K	0.12±0.04	>M1
728.7**	Pt	K		(M1)
			0.030±0.010	
729.6	Pt	K		M1
749.8	Pt	K		
			0.017±0.009	
751.0	Pt	K		M1,M1+E2
763.3	Pt	K		M1,M1+E2
			0.011±0.006	
764.5	Pt	K		
774.6	Pt	K		
			0.014±0.007[a)]	
775.5**	Pt	K		
782.6	Pt	K		
			0.007±0.003	
783.7	Pt	K		E2(+M1)
787.4	Pt	K	0.031±0.010	M1
789.2	Pt	K	0.055±0.010	>M1
792.2	Pt	K	0.018±0.009	M1(+E2)
868.4	Pt	K	0.022±0.007	M1
903.5	Pt	K		>M1
			0.024±0.006	
904.9	Pt	K		
905.7	Ir	K	0.015±0.004	M1
920.5	Pt	K		
			0.007±0.002	
917.7	Ir	K		
926.8	Pt	K		
			0.012±0.004	
928.5	Pt	K		(M1+E2)
999.7	Pt	K	0.009±0.004	M1+E2
1007.8**	Pt	K	0.015±0.003	M1
1102.1	Pt	K	no γ	>M1
1158.5	Pt	K	≈0.0013	E1
1215.5	Pt	K	≈0.0037	E2
1245.0	Pt	K		
			0.027±0.009	
1246.8	Pt	K		>M1
1309.2*	Pt	K		>M1
			0.014±0.006	
	Ir	K		
1372.1**	Pt	K	0.004±0.002	M1+E2
1393.1	Pt	K	0.0083±0.002	M1
1407.8	Ir	K	≈0.0012	E1
1426.6	Pt	K	0.006±0.003	M1
1587.0	Ir	K	0.0022±0.0010	E2(+M1)
1798.1	Pt	K	0.0006±0.0002	E1
1807.8**	Pt	K	0.0007±0.0002	E1
1960.0	Pt	K	0.0010±0.0003	E2
1965.9	Pt	K		E2
			0.0012±0.0004	
1968.4	Pt	K		(E2)
2005.6	Pt	K	0.0010±0.0004	E2
2022.4	Pt	K	0.0011±0.0003	E2
2043.1	Pt	K	0.0014±0.0006	E2+M1
2126.5	Pt	K	0.0012±0.0005	E2(+M1)

TABLE 6

E(keV)	Nucleus	α_K	$R=\alpha_K/\alpha_K(M1)$
583.	Pt	$\gtrsim 0.20$	$\gtrsim 4.2$
668.5	Pt	0.11 ± 0.04	3.3
709.0	Pt	>0.13	>4.8
789.2	Pt	0.055 ± 0.010	2.6
903.5	Pt	>0.024	>1.6
1102.1	Pt	>0.13	>15
1246.8	Pt	>0.027	>4.1
1309.2	Pt	>0.073	>12.8
713.7	Ir	0.12 ± 0.04	4.4

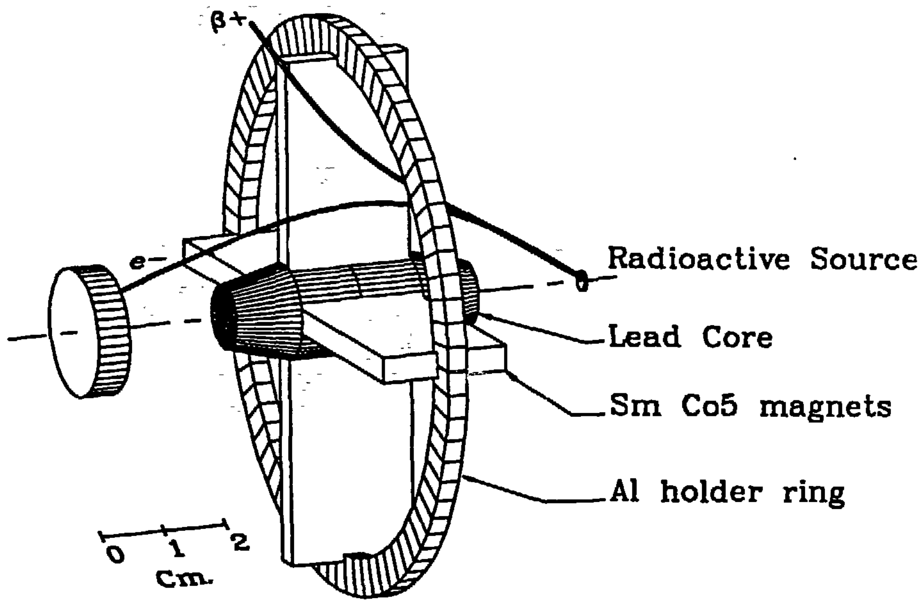
β+
e−
Radioactive Source
Lead Core
Sm Co5 magnets
Al holder ring
0
1
2
Cm.

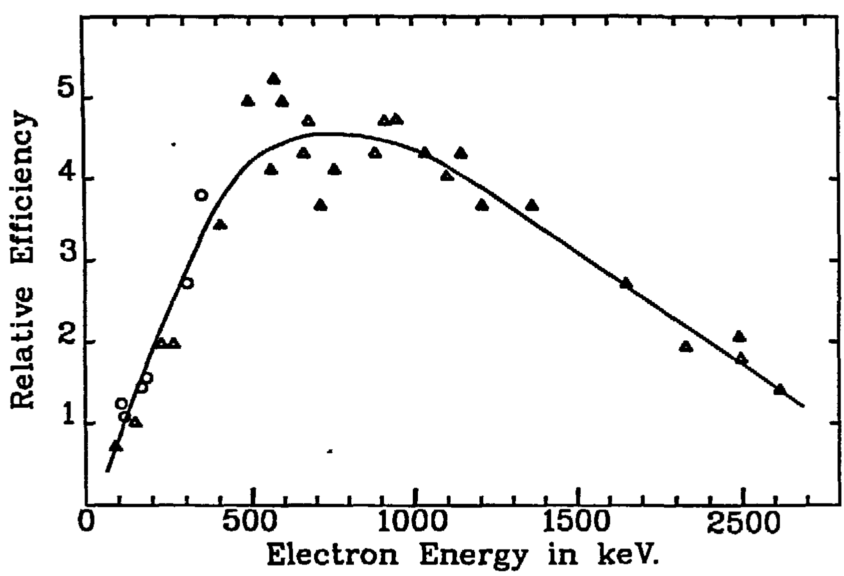
Relative Efficiency
1
2
3
4
5
0
500
1000
1500
2500
Electron Energy in keV.

Fig. 1

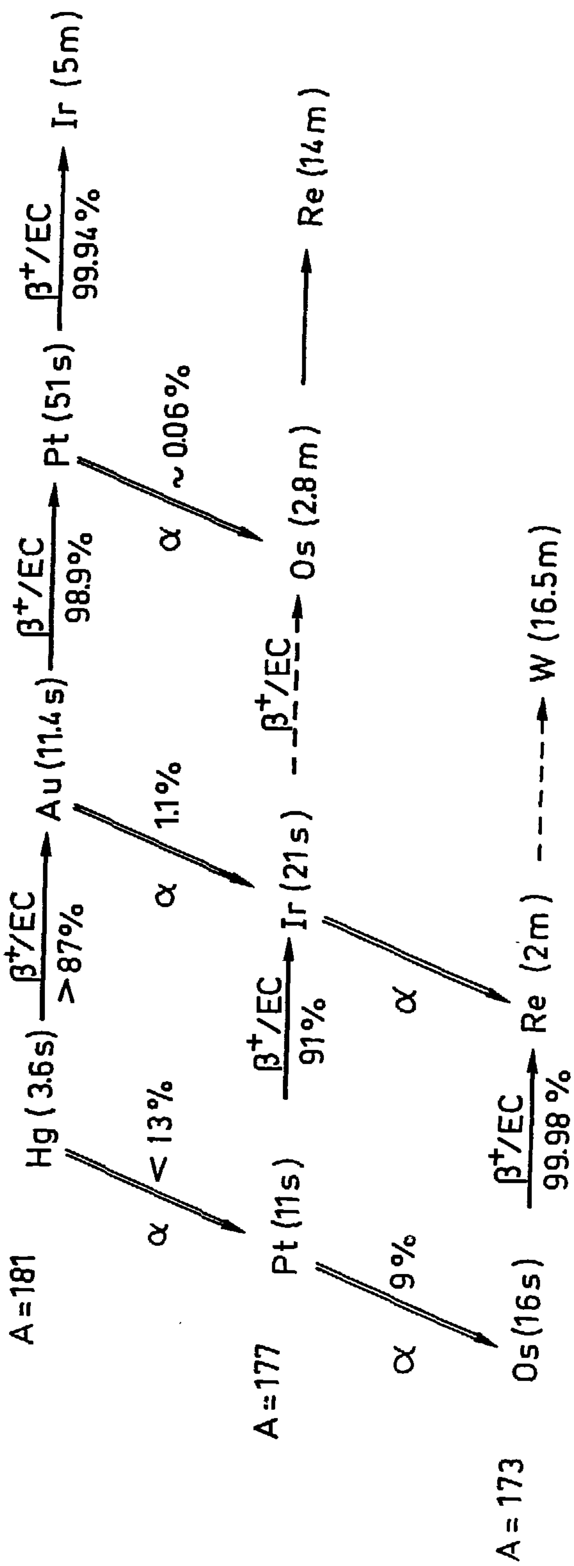
A = 181
A = 177
A = 173
Hg (3.6s)
β+/EC
>87%
Au (11.4 s)
β+/EC
98.9%
Pt (51s)
β+/EC
99.94%
Ir (5m)
α
< 13%
α
1.1%
α
~ 0.06%
Pt (11s)
β+/EC
91%
Ir (21s)
β+/EC
Os (2.8m)
Re (14m)
α
9%
α
Os (16s)
β+/EC
99.98%
Re (2m)
W (16.5m)

Fig. 2

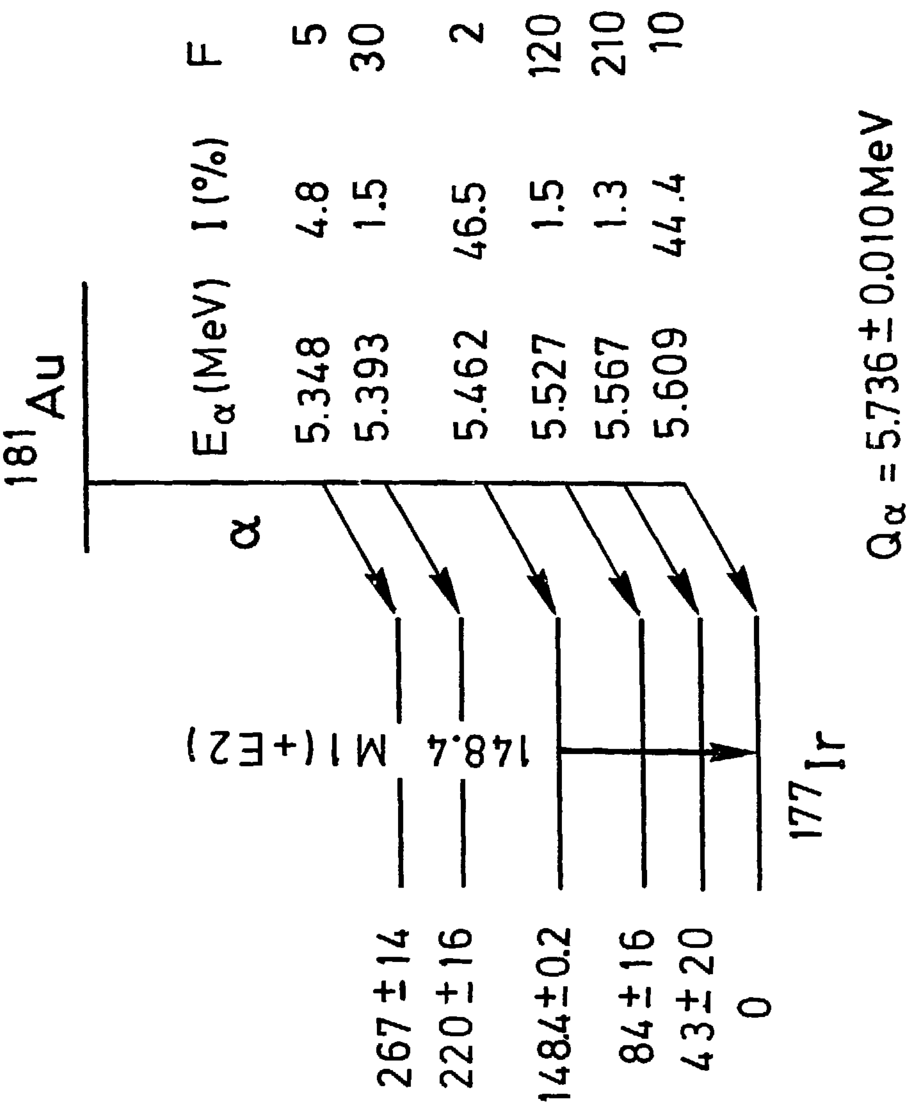
181Au
α
Eα (MeV) I (%) F
5.348 4.8 5
5.393 1.5 30
5.462 46.5 2
5.527 1.5 120
5.567 1.3 210
5.609 44.4 10
Qα = 5.736 ± 0.010 MeV
148.4 M1(+E2)
177Ir
267 ± 14
220 ± 16
148.4 ± 0.2
84 ± 16
43 ± 20
0

Fig. 3

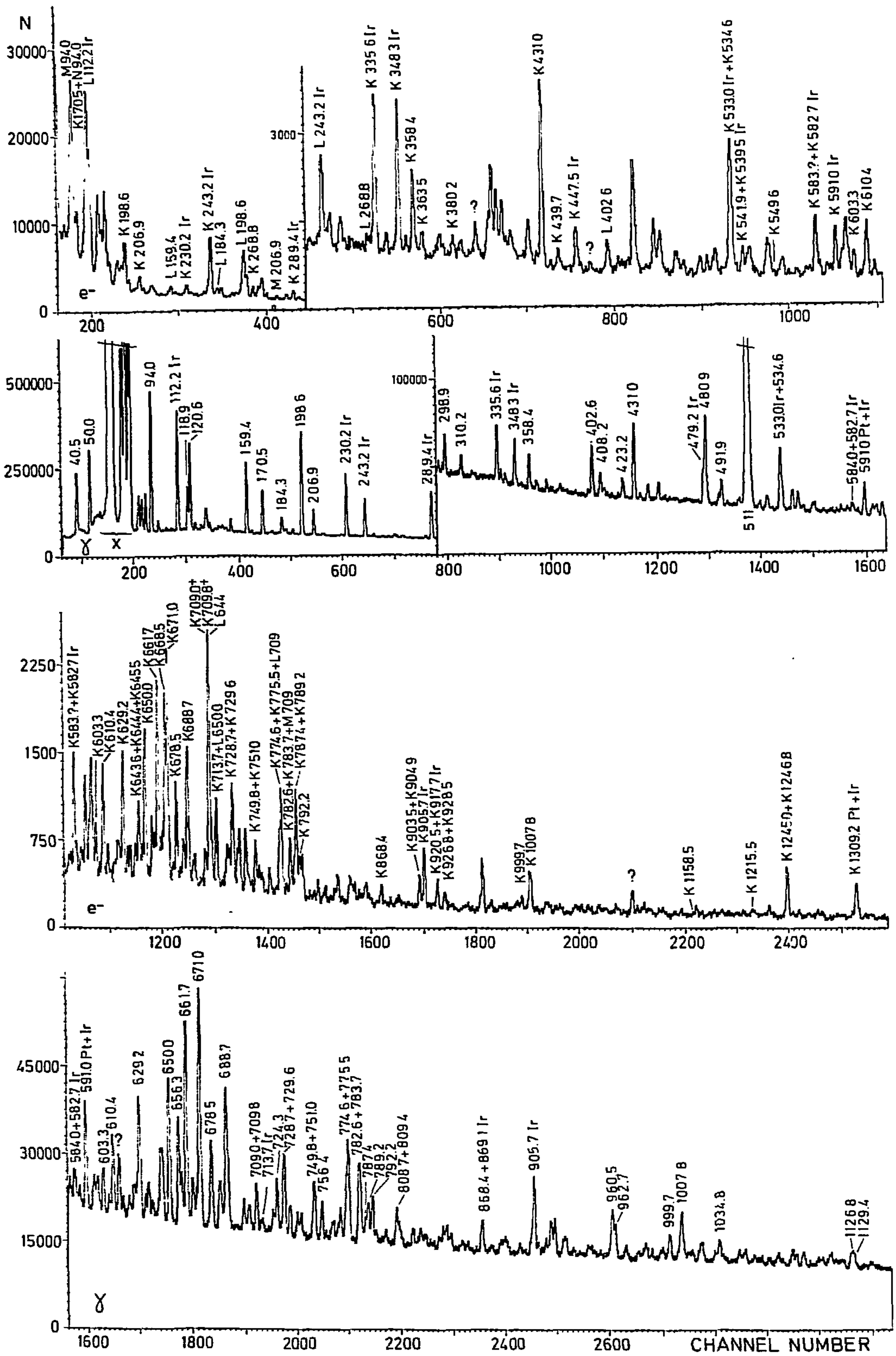
N
30000
20000
10000
0
200
400
600
800
1000
e⁻
500000
250000
0
200
400
600
800
1000
1200
1400
1600
γ
X
2250
1500
750
0
1200
1400
1600
1800
2000
2200
2400
e⁻
45000
30000
15000
0
1600
1800
2000
2200
2400
2600
CHANNEL NUMBER
γ

Fig. 4a

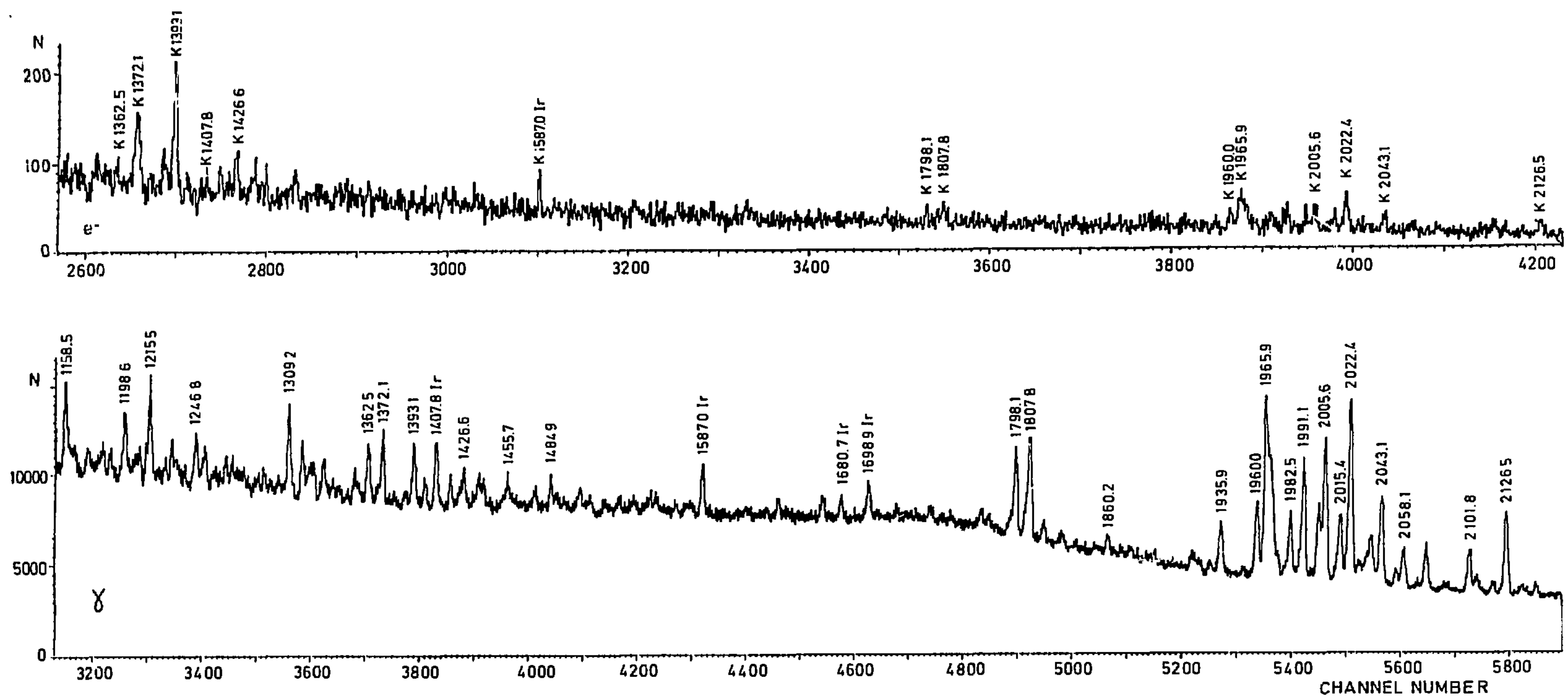
N
200
100
0
e⁻
K 1362.5
K 1372.1
K 1393.1
K 1407.8
K 1426.6
K 1587.0 Ir
K 1798.1
K 1807.8
K 1960.0
K 1965.9
K 2005.6
K 2022.4
K 2043.1
K 2126.5
2600
2800
3000
3200
3400
3600
3800
4000
4200
N
10000
5000
0
γ
1158.5
1198.6
1215.5
1246.8
1309.2
1362.5
1372.1
1393.1
1407.8 Ir
1426.6
1455.7
1484.9
1587.0 Ir
1680.7 Ir
1698.9 Ir
1798.1
1807.8
1860.2
1935.9
1960.0
1965.9
1982.5
1991.1
2005.6
2015.4
2022.4
2043.1
2058.1
2101.8
2126.5
3200
3400
3600
3800
4000
4200
4400
4600
4800
5000
5200
5400
5600
5800
CHANNEL NUMBER

Fig. 4 b

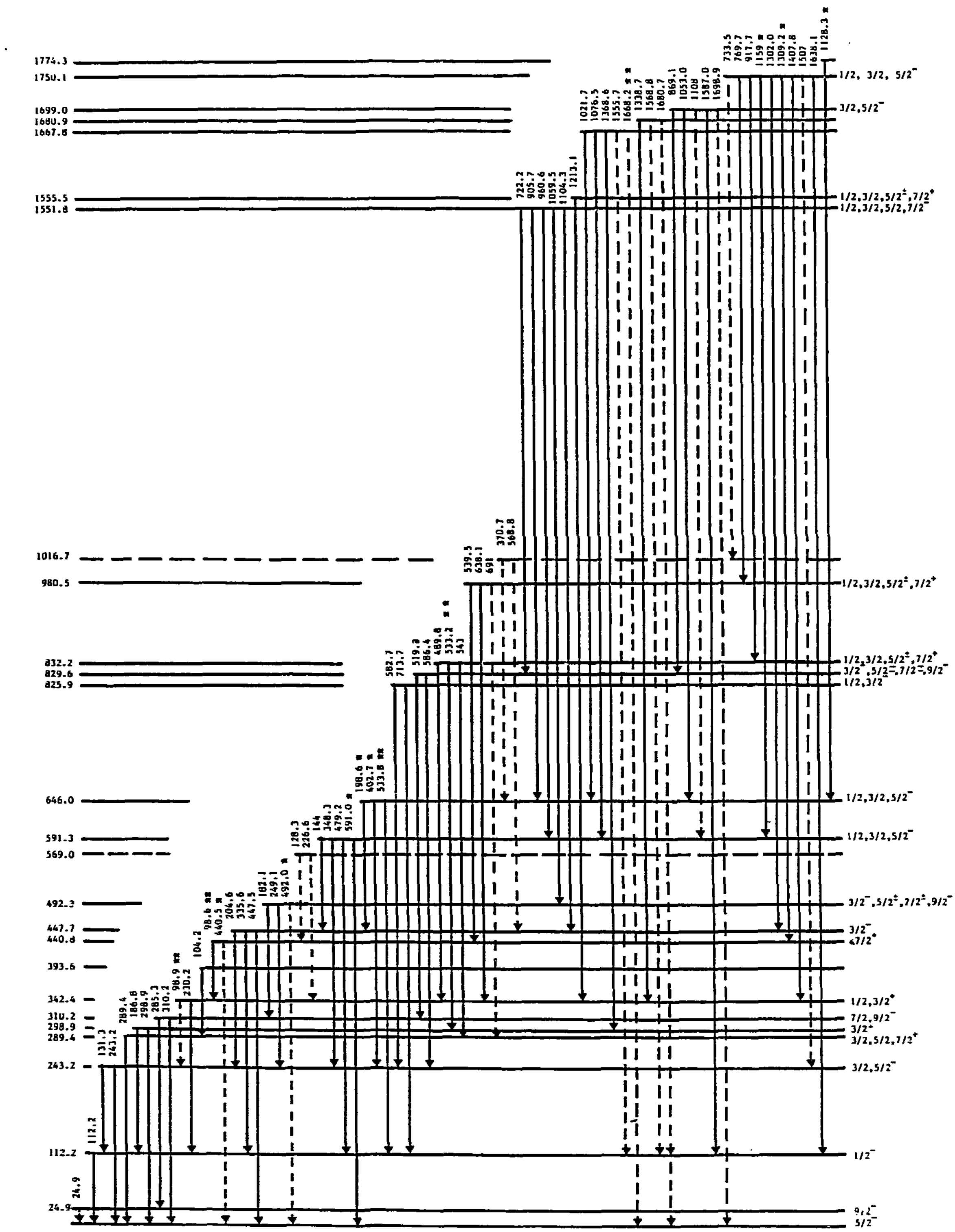
1774.3
1750.1
1699.0
1680.9
1667.8
1555.5
1551.8
1016.7
980.5
832.2
829.6
825.9
646.0
591.3
569.0
492.3
447.7
440.8
393.6
342.4
310.2
298.9
289.4
243.2
112.2
24.9
1/2, 3/2, 5/2⁻
3/2,5/2⁻
1/2,3/2,5/2±,7/2⁺
1/2,3/2,5/2,7/2⁻
1/2,3/2,5/2±,7/2⁺
1/2,3/2,5/2±,7/2⁺
1/2,3/2
1/2,3/2,5/2⁻
1/2,3/2,5/2⁻
3/2⁻,5/2±,7/2±,9/2⁻
3/2⁻
7/2,9/2⁻
3/2⁺
3/2,5/2,7/2⁺
3/2,5/2⁻
1/2⁻
9/2⁻
5/2⁻

Fig. 5

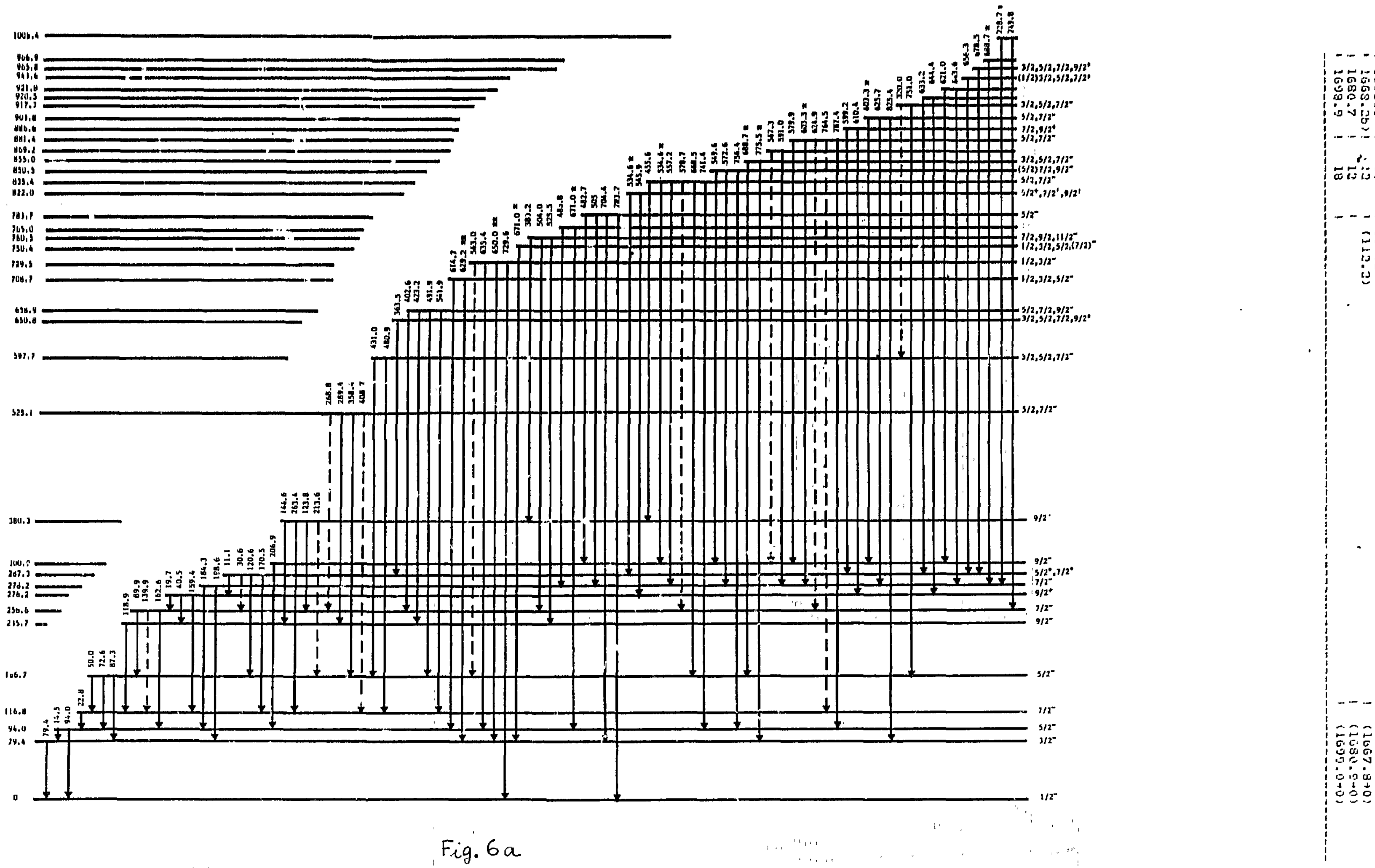

Fig. 6a

527.8	4.7	(c)		
531	weak	120.6,(170.5),(637.5),656.3		1474.3 → 943.6
534.6*	≈ 50 **	(50.0),(118.9),120.6,159.4,170.5,206.9,460.0,(595.9),1263,1273	{	832.0 → 287.3 (835.4 → 300.9)

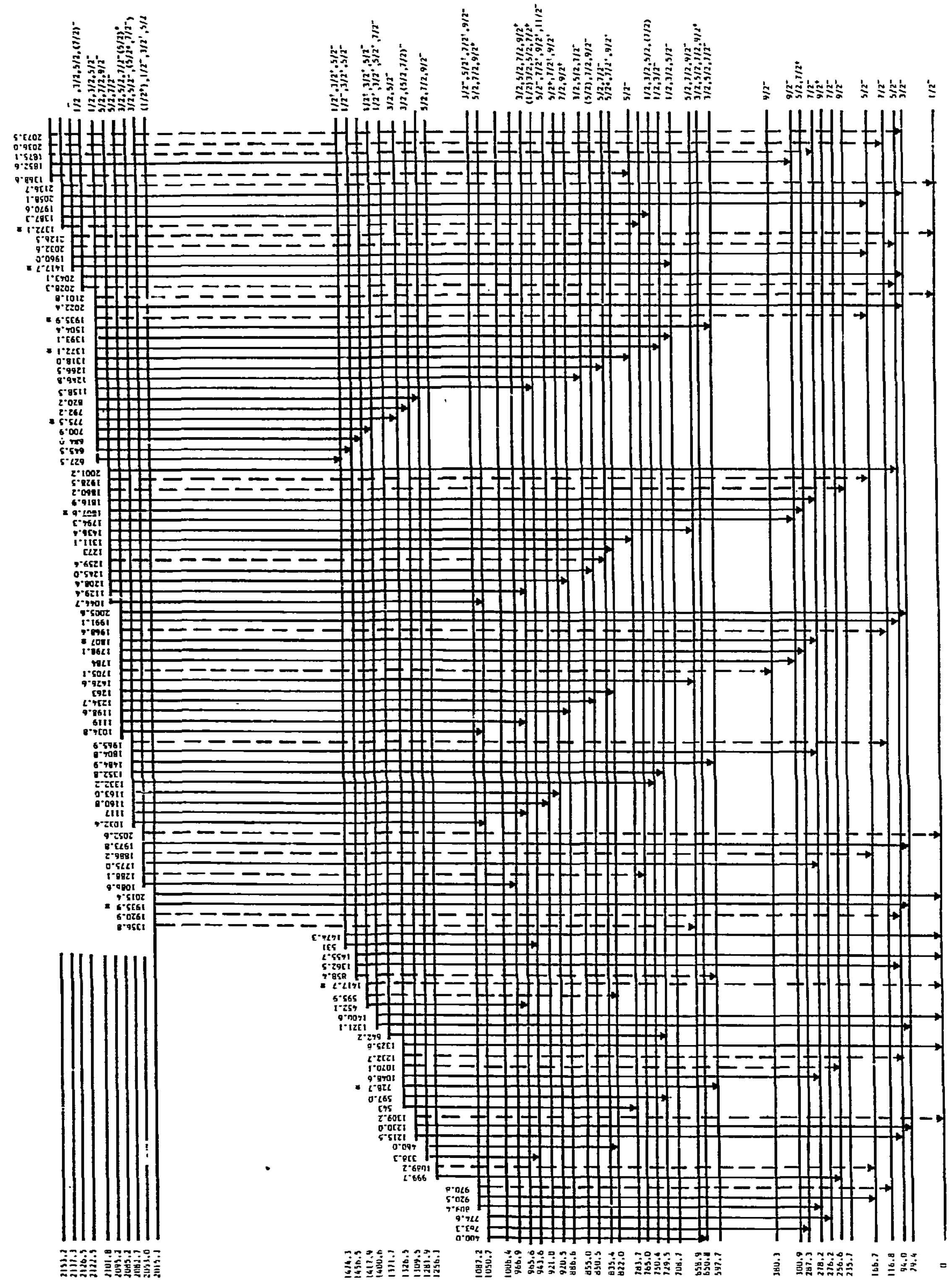

Fig. 6b

820.2	14	(50.0),12 .6, 5 . , .5, . , . ,	
823.8	3.4	(c)	903.8 → 79.4
825.4	13	79.4	
834.9	10	(c)	
838.7	7.0	(c)	

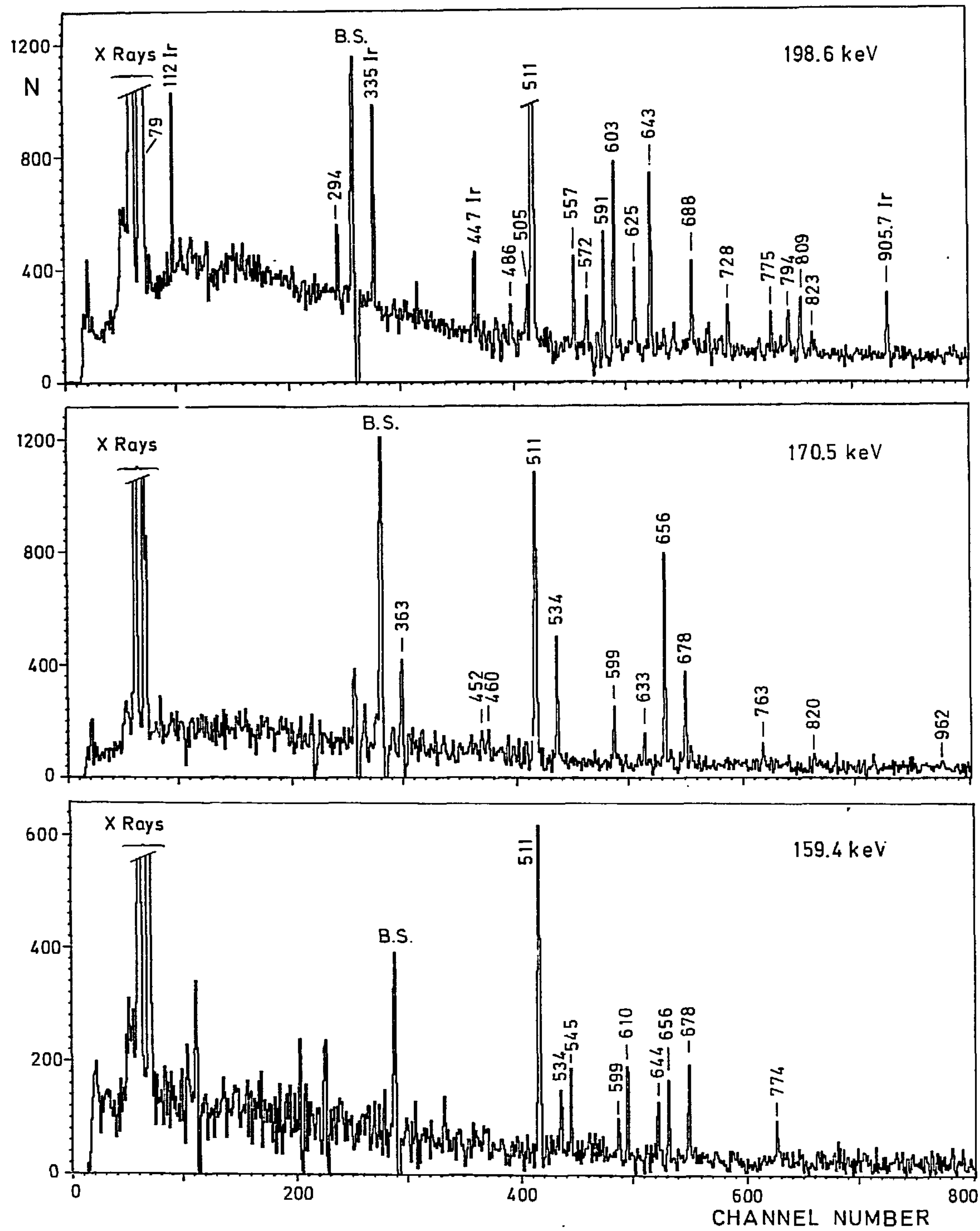

Fig. 7a

334.8 !	6.2 !	94.0,666.1
342.5 !	8.0 !	(c)
348.4 !	5.2 !	(c)
352.8 !	16 !	94.0,635.4,650.0,729.6
356.8 !	8.7 !	

2082.7 → 729.5
(2015.3 → 658.9)

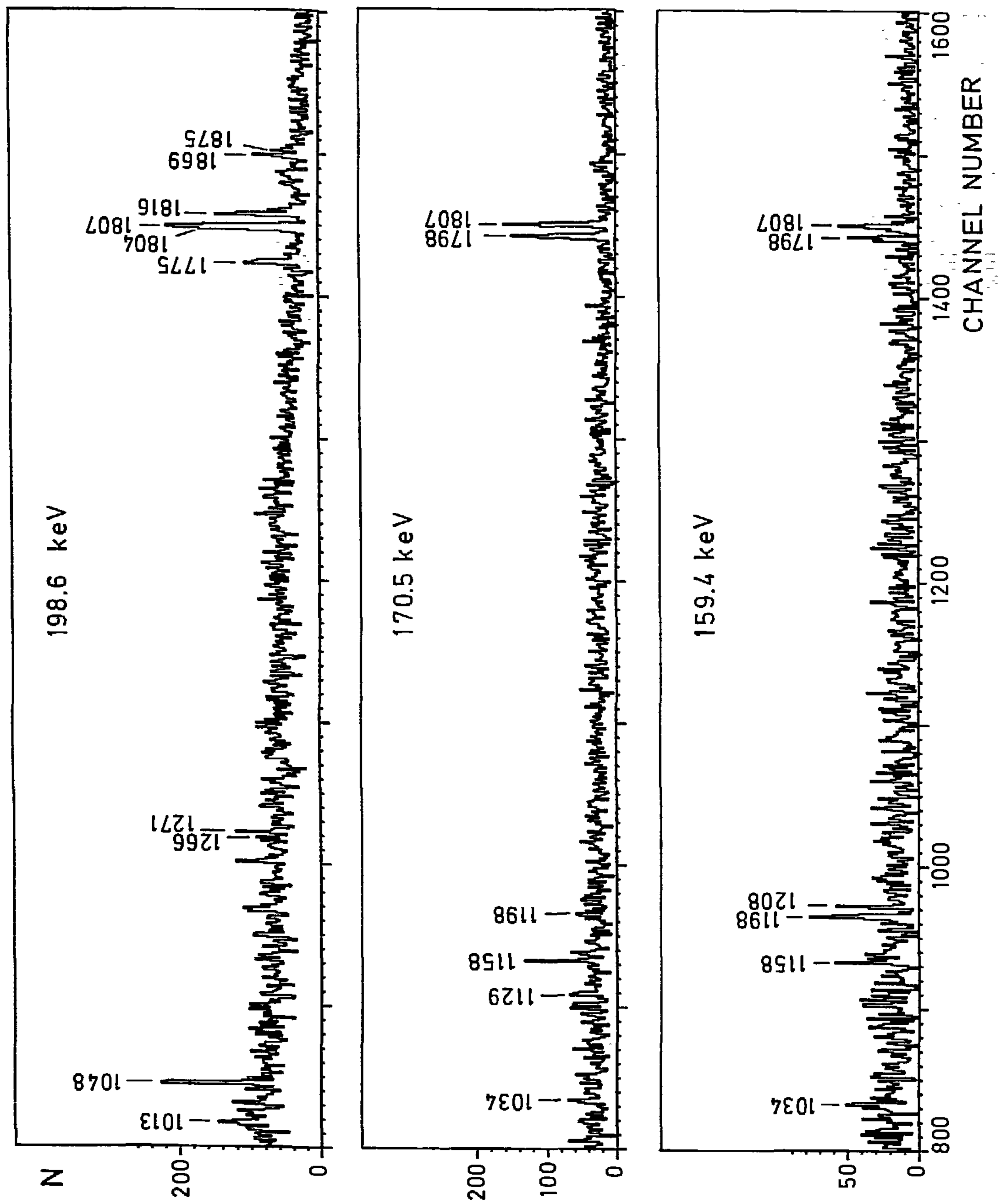

2126.5	110		(2137.3
2136.7	12		
2140.2	6.2	(c)	
2146.4	16	(c)	

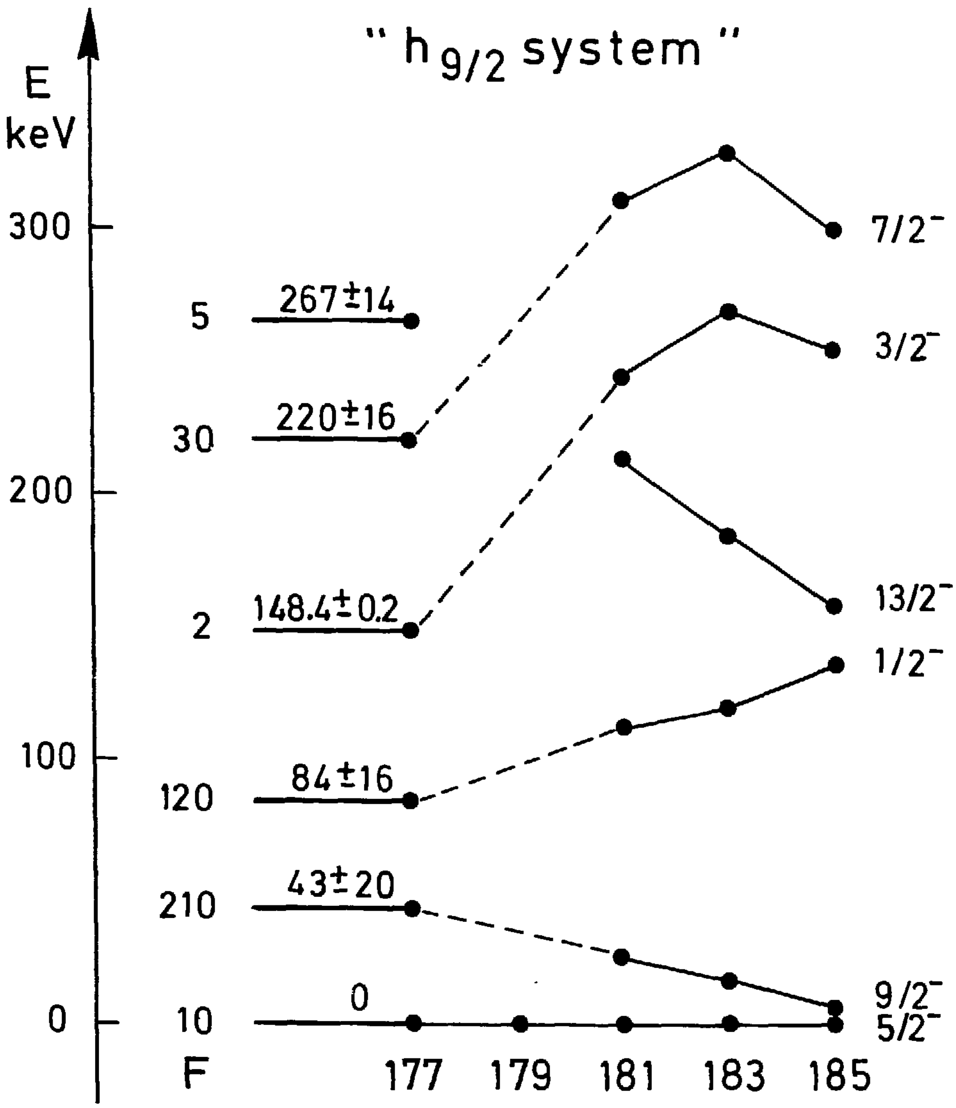

Fig. 8

			0.11 ± 0.04	M1
668.5	Pt	K	0.023±0.010	M1+E2
671.0**	Pt	K	0.020±0.009	M1+E2
678.5	Pt	K	0.024±0.010	M1(+E2)
688.7**	Pt	K		

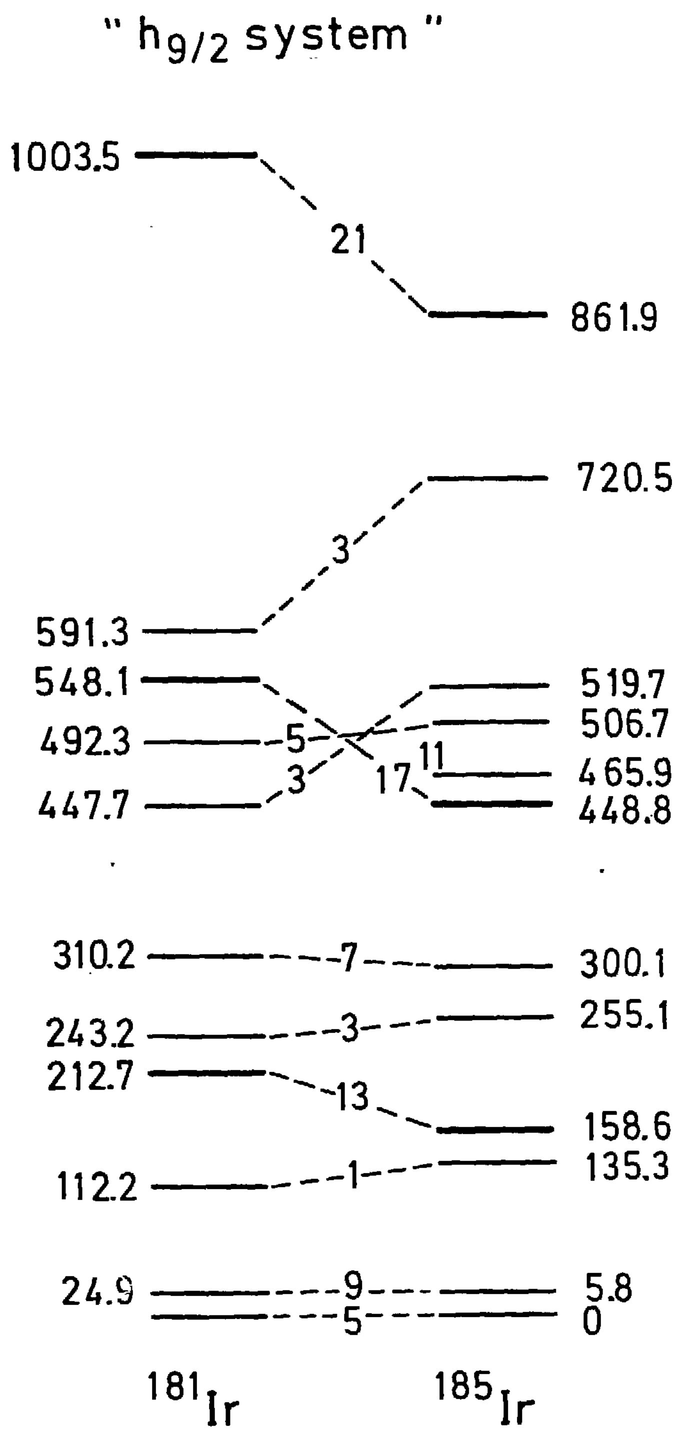

Fig. 9

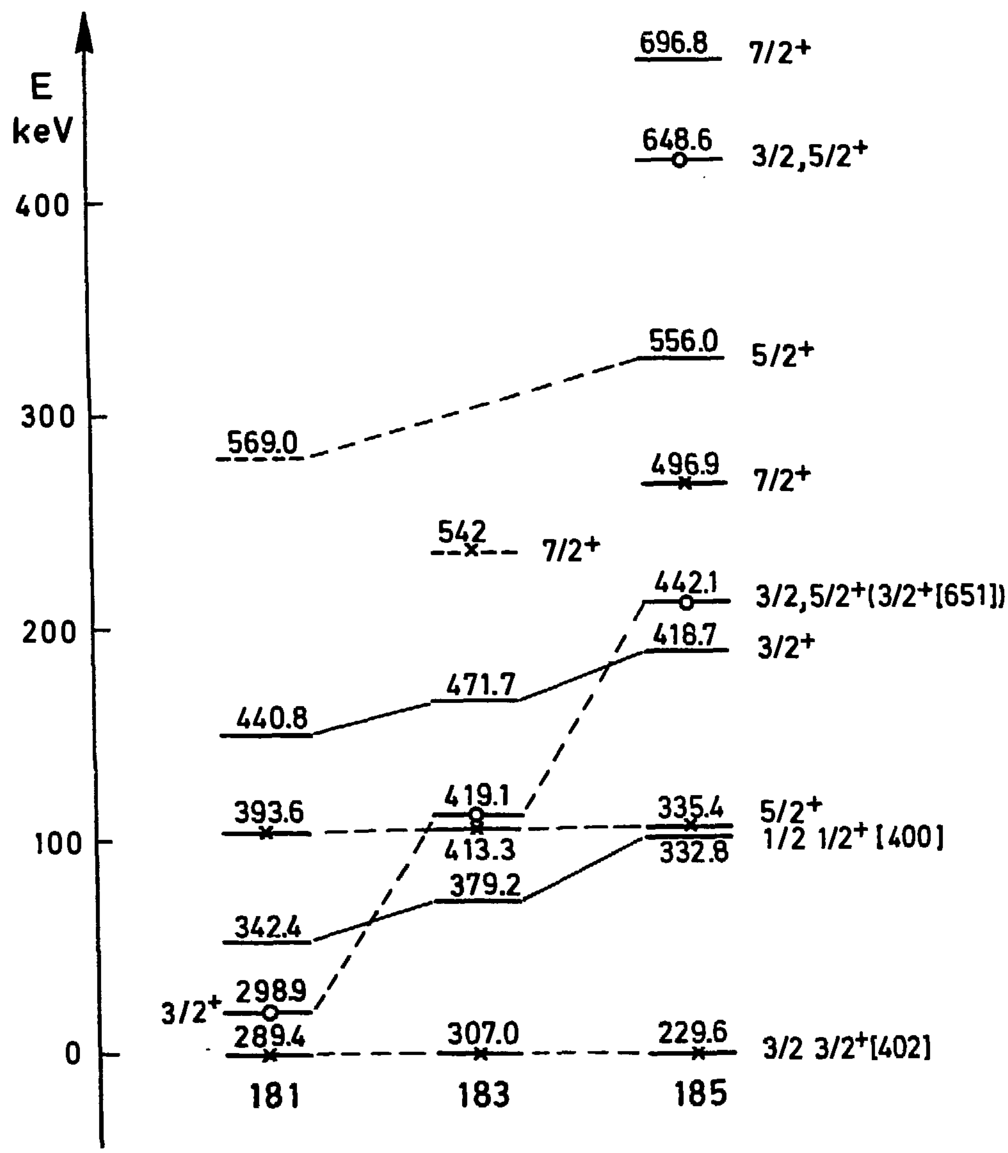
E
keV
400
300
200
100
0
696.8 7/2+
648.6 3/2,5/2+
556.0 5/2+
569.0
496.9 7/2+
542 7/2+
442.1 3/2,5/2+(3/2+[651])
418.7 3/2+
471.7
440.8
393.6
419.1
413.3
335.4 5/2+
332.8 1/2 1/2+ [400]
379.2
342.4
3/2+ 298.9
289.4
307.0
229.6 3/2 3/2+[402]
181
183
185

Fig. 10

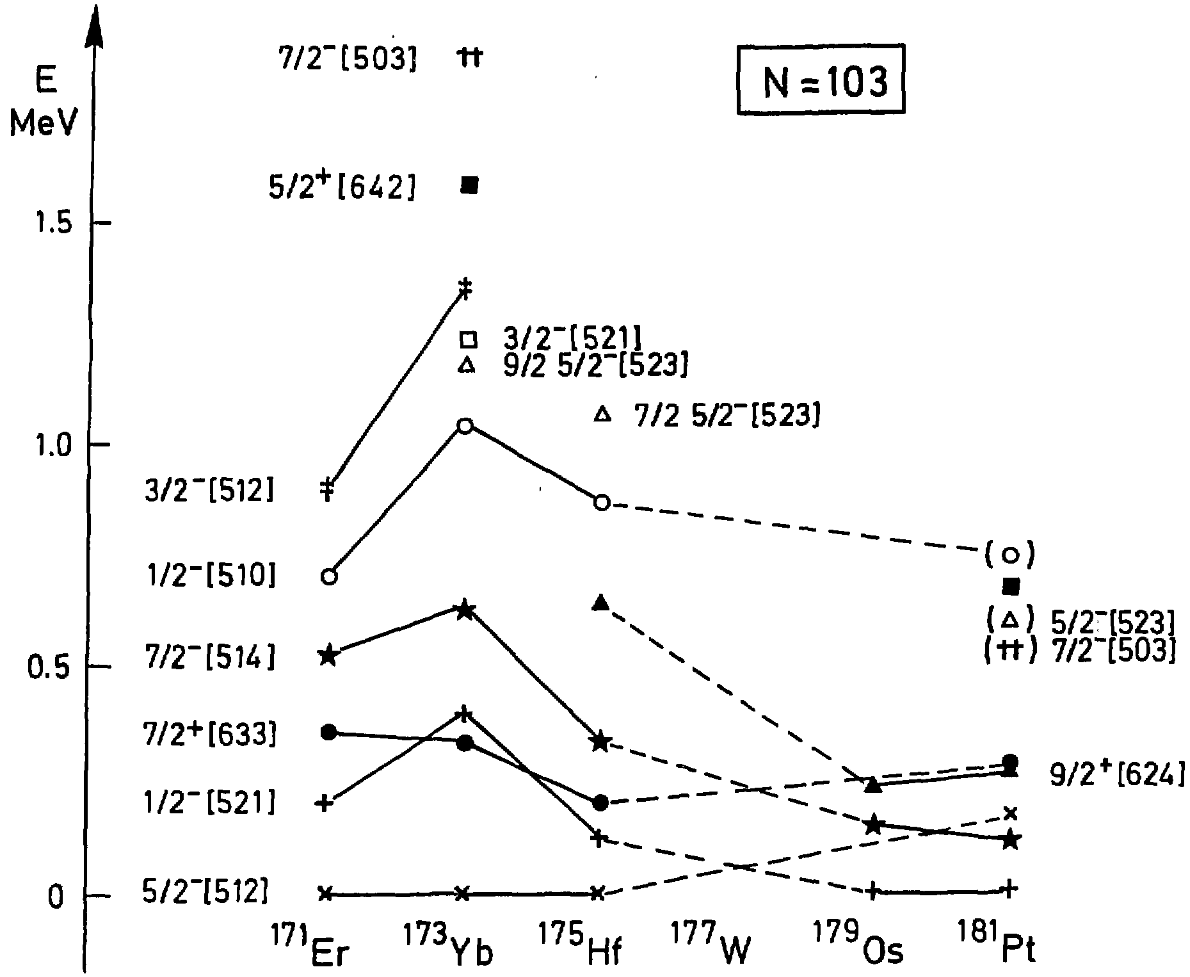

E
MeV
1.5
1.0
0.5
0
N = 103
7/2⁻[503]
5/2⁺[642]
3/2⁻[521]
9/2 5/2⁻[523]
7/2 5/2⁻[523]
3/2⁻[512]
1/2⁻[510]
7/2⁻[514]
7/2⁺[633]
1/2⁻[521]
5/2⁻[512]
5/2⁻[523]
7/2⁻[503]
9/2⁺[624]
171Er
173Yb
175Hf
177W
179Os
181Pt

Fig. 11

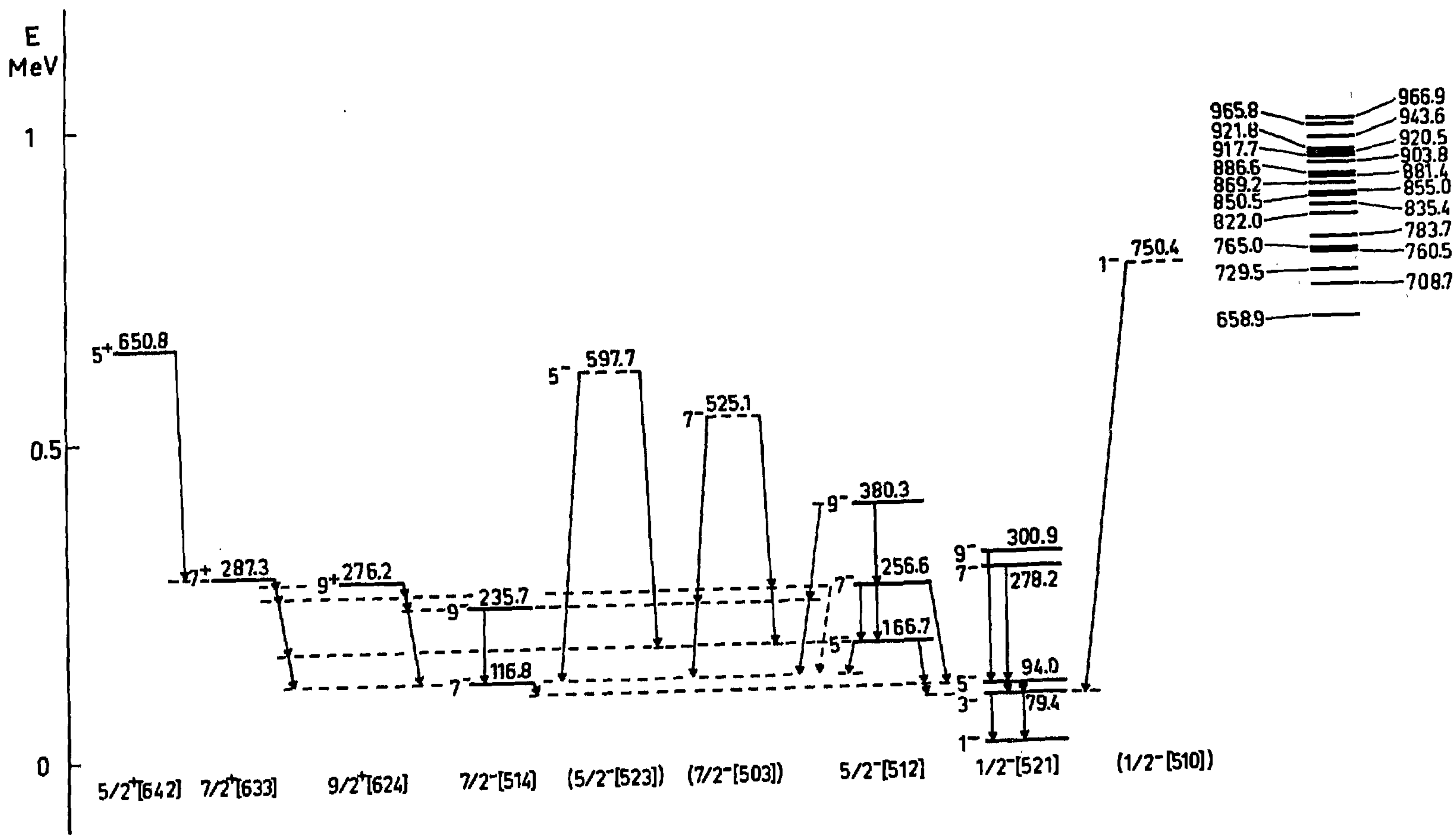
E
MeV
1
0.5
0
5+ 650.8
7+ 287.3
9+ 276.2
9- 235.7
7- 116.8
5- 597.7
7- 525.1
9- 380.3
7- 256.6
5- 166.7
9- 300.9
7- 278.2
5- 94.0
3- 79.4
1-
1- 750.4
965.8
921.8
917.7
886.6
869.2
850.5
822.0
765.0
729.5
658.9
966.9
943.6
920.5
903.8
881.4
855.0
835.4
783.7
760.5
708.7
5/2+[642]
7/2+[633]
9/2+[624]
7/2-[514]
(5/2-[523])
(7/2-[503])
5/2-[512]
1/2-[521]
(1/2-[510])

Fig. 12

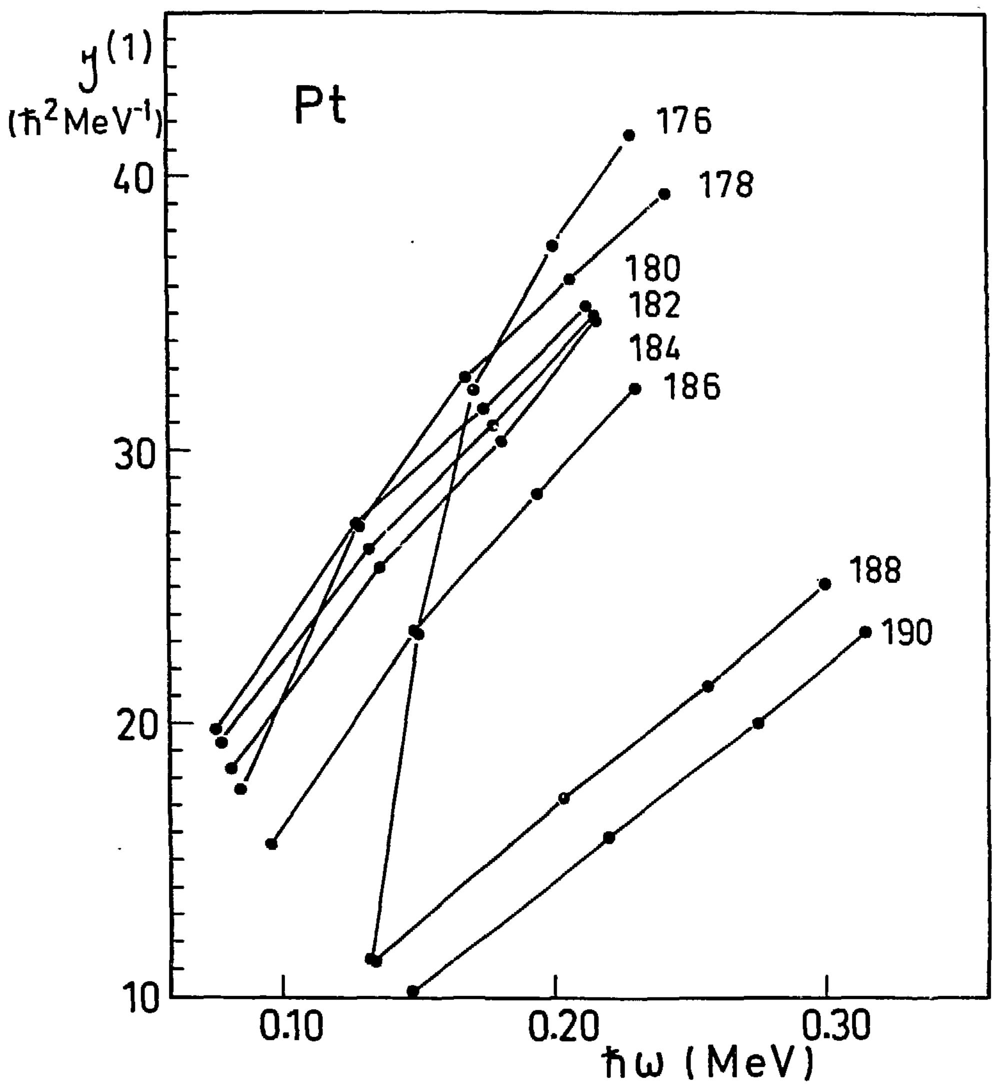

$\mathcal{J}^{(1)}$
($\hbar^2$MeV^{-1})
Pt
176
178
180
182
184
186
188
190
40
30
20
10
0.10
0.20
0.30
$\hbar\omega$ (MeV)

Fig. 13